Climate Vulnerability Assessment of Salt Lake City's Water Systems

Year 5 Report

Prepared by:

Dr. Court Strong and Luke Stone
Department of Atmospheric Sciences
University of Utah

Dr. Paul Brooks, Meg Wolf,
Logan Jamison, and Baylee Olds
Department of Geology and Geophysics
University of Utah

Dr. Steve Burian, Dr. Ryan
Johnson and Danyal Aziz,
Department of Civil, Construction,
and Environmental Engineering
University of Alabama

THE UNIVERSITY OF UTAH

THE UNIVERSITY OF ALABAMA

Table of Contents

1. Introduction

This report presents findings from research conducted during Year 5 of the project "Climate Vulnerability Assessment of Salt Lake City's Water System." The Salt Lake City Department of Public Utilities (SLCDPU) recommended an overarching goal structure for the project responsive to an expressed need for climate readiness tools delivered by the University of Utah (UU) team meeting the set of priority research objectives included in the Year 5 statement of work:

Objective 1. *Climate: Seasonal to multi-year precipitation guidance*. (a) Conduct global climate model experiments to understand how the Atlantic driver of precipitation interacts with El Niño. (b) Develop a tool for seasonal to multi-year precipitation guidance.

Objective 2. *Hydrology: Tool development and resolving key knowledge gaps identified during years 1-4*. (a) Develop clear tools in consultation with SLCDPU staff that translate research findings into operations. (b) Resolve key remaining knowledge gaps underlying the statistical model of streamflow.

Objective 3. *Engineering: Supporting system operations with supply and demand management guidance.* (a) Develop a workflow to use drought severity-duration-frequency (SDF) curves for analysis of vulnerabilities of the water system to low-flow scenarios. (b) Develop water system management and guidance tools (demand) in collaboration with hydrology (seasonal supply) and climate (annual supply) to enhance resilience.

Research conducted by the coordination between the UU and UA teams in achieving these objectives led to three key scientific discoveries which inform the order and format of results presented here, and also motivate directions for future research. We briefly summarize the discoveries here and detail them in subsequent sections of the report:

Key Discovery 1. (Climate) Atlantic Ocean surface temperature drives multi-year precipitation anomalies which are crucial to baseflow and water yield. The Atlantic-driven atmospheric pattern shifts the precipitation anomalies associated with El Niño north-south, providing potential for predictability on seasonal to three-year time scales. A 10,000 perpetual current-climate simulation with the Geophysical Fluid Dynamics Lab (GFDL) global climate model confirms the role of the AQM in shifting the ENSO precipitation pattern north-south.

Key Discovery 2. (Hydrology) New analyses during year 5 focused on two knowledge gaps underlying our statistical model of streamflow. First, targeted streamflow sampling for chemistry and isotopes, including leveraged funding for ^3H sampling, identified a strong relationship between groundwater age and runoff efficiency in SLCDPU catchments. These observations are consistent with our recharge model that suggests groundwater storage is strongly related to multiple years of antecedent precipitation and melt dynamics (Year 4). Groundwater ages range from 4 to 20 years supporting our inferences that streamflow in any one year is the product of multiple years of antecedent climate. Second, the finding that faster melt is positively related to both spring streamflow and groundwater recharge suggests that faster (slower) melt minimizes (increases) sublimation and evaporation losses. These changes during the winter and spring are likely to decrease runoff efficiency in the future. We have begun initial analyses to determine both the magnitude and spatial variability of these losses.

Key Discovery 3. (Engineering) Mean air temperature and cumulative precipitation during April and May exhibit a strong correlation to total seasonal water use and water system performance spanning April to October. Univariate frequency analysis can address the practical knowledge gap in terms of the lack of usable multi-year streamflow deficit information for urban water supply systems' operational planning and management.

The next three sections detail the scientific discoveries and new modeling capabilities developed in pursuit of the three research objectives (Sections 2-4). Section 5 presents initial efforts to synthesize these findings and modeling capabilities into a framework for supporting water resource decision-making on seasonal and longer time scales.

2. Climate: Deeper investigation of Atlantic Driver of Groundwater Recharge

Previously we identified two modes of coupled variability that link Atlantic sea surface temperatures and western US precipitation. This analysis focused on the northern Atlantic Ocean sea surface temperatures and a three-year window. To better understand the seasonal impact of the Atlantic on wet and dry years in the study area, we expanded the domain to global sea surface temperatures and focused on a one-year time frame.

Key discoveries:

- Study-region hydroclimate is affected by interactions between the Atlantic Quadpole Mode (AQM) and the El Niño - Southern Oscillation (ENSO).
- The AQM shifts the precipitation anomalies associated with ENSO north-south, providing overall wetter conditions during warm AQM and drier conditions during cold AQM.
- A 10,000 perpetual current-climate simulation with the Geophysical Fluid Dynamics Lab (GFDL) global climate model confirms the role of the AQM in shifting the ENSO precipitation pattern north-south.

Key tool

- A lookup table was developed to predict winter precipitation percent anomalies associated with different combinations of ENSO and the AQM.

2.1 Atlantic Quadpole Mode and Seasonal Precipitation

Using maximum covariance analysis (MCA), a statistical method which finds the most important coupled modes of variability among two variables in a large data set, we identified the two most significant modes of coupled variability between precipitation and sea surface temperatures.

In observations, the first mode of coupled variability, referred to as MCA1, is the familiar ENSO pattern in which positive MCA1 corresponds to El Niño with elevated central tropical Pacific SSTs (Figure 2.1a) and a dry-north / wet-south precipitation dipole over the western U.S. (Figure 2.1c). This mode accounts for 59% of the total covariation between Atlantic sea surface temperature and western US precipitation. To illustrate the associated atmospheric pattern, we show 300-hPa geopotential height (Z_{300}) in Figure 2.1b, which can be interpreted similarly to a weather map of sea level pressure (e.g., El Niño corresponds to anomalously low Z_{300} which overlies anomalously low sea level pressure in the Gulf of Alaska, and La Niña corresponds to the reverse). The Z_{300} pattern shows the canonical poleward and eastward propagating atmospheric wave associated with central tropical Pacific storminess, producing a strong trough (low-pressure area) in the northeast Pacific responsible for the positive precipitation anomalies in the Southwest during the ENSO warm phase. The associated time series of SST ($S1$) and precipitation ($P1$) reflect strong interannual variability (Figure 2.1d).

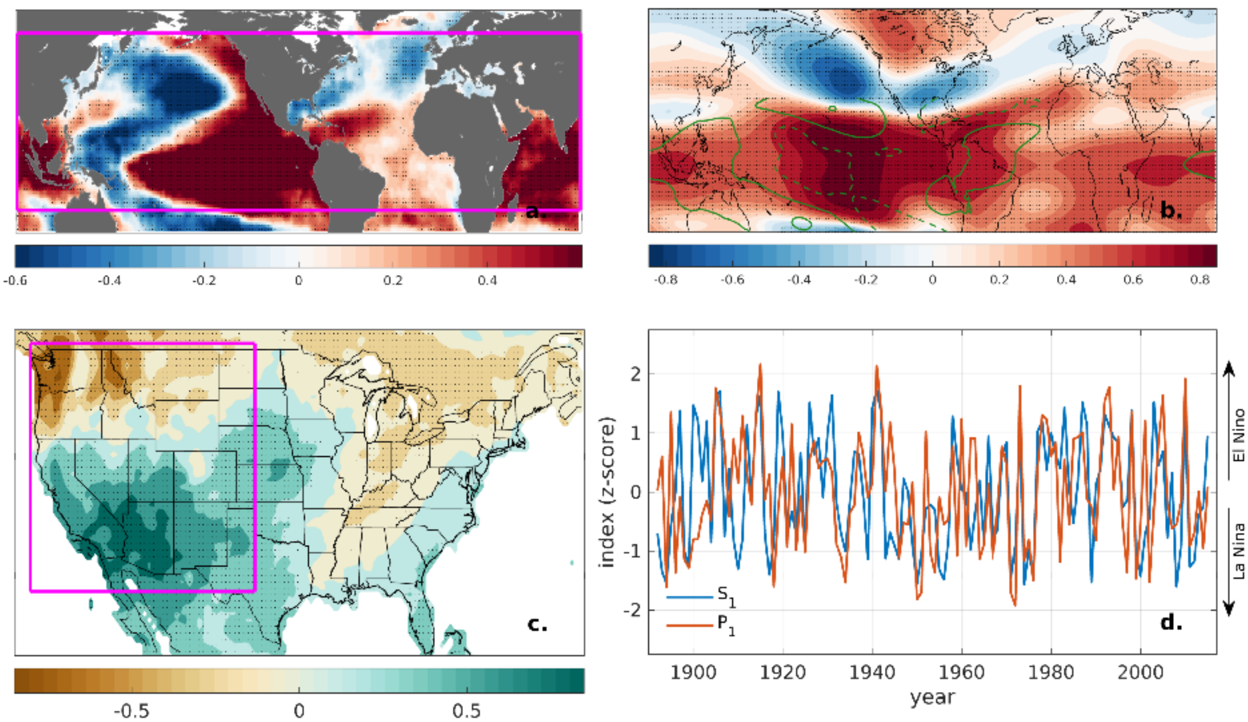

Figure 2.1. Based on Maximum Covariance Analysis (MCA), the leading mode of coupled variability (MCA1) between sea surface temperatures and western-US precipitation. The upper left map shows how sea surface temperatures correlate with the MCA1 mode, and the lower left map shows how precipitation correlates with the MCA1 mode. When the MCA1 sea surface temperature index and MCA1 precipitation index (panel d) are both above average, the anomalies of sea surface temperature and precipitation closely resemble the patterns mapped at left. When the indices are both below average, the anomalies of sea surface temperature and precipitation are the reverse of those shown at the lower left. The magenta boxes in the maps at left indicate the SST and precipitation analysis domains used in the MCA. In panel b at upper right, shading shows how 300-hPa geopotential height correlates with MCA1 (can be interpreted similarly to a weather map showing pressure), dashed green contours indicate regions of enhanced tropical storminess, and solid green contours indicate regions of reduced tropical storminess.

The second coupled mode, MCA2, accounts for variability most strongly in the Atlantic (Figure 2.2a) and accounts for 23% of the total covariation between Atlantic sea surface temperature and western US precipitation. Here, we refer to MCA2 as the Atlantic Quadpole Mode (AQM), where *S2* > 0 is the Warm AQM and *S2*< 0 is the Cold AQM (Figure 2.2d). AQM captures precipitation variability across much of the coastal and Intermountain U.S., including where the study region lies, in the transition zone between the wet and dry anomalies associated with ENSO (Figure 2.2c).

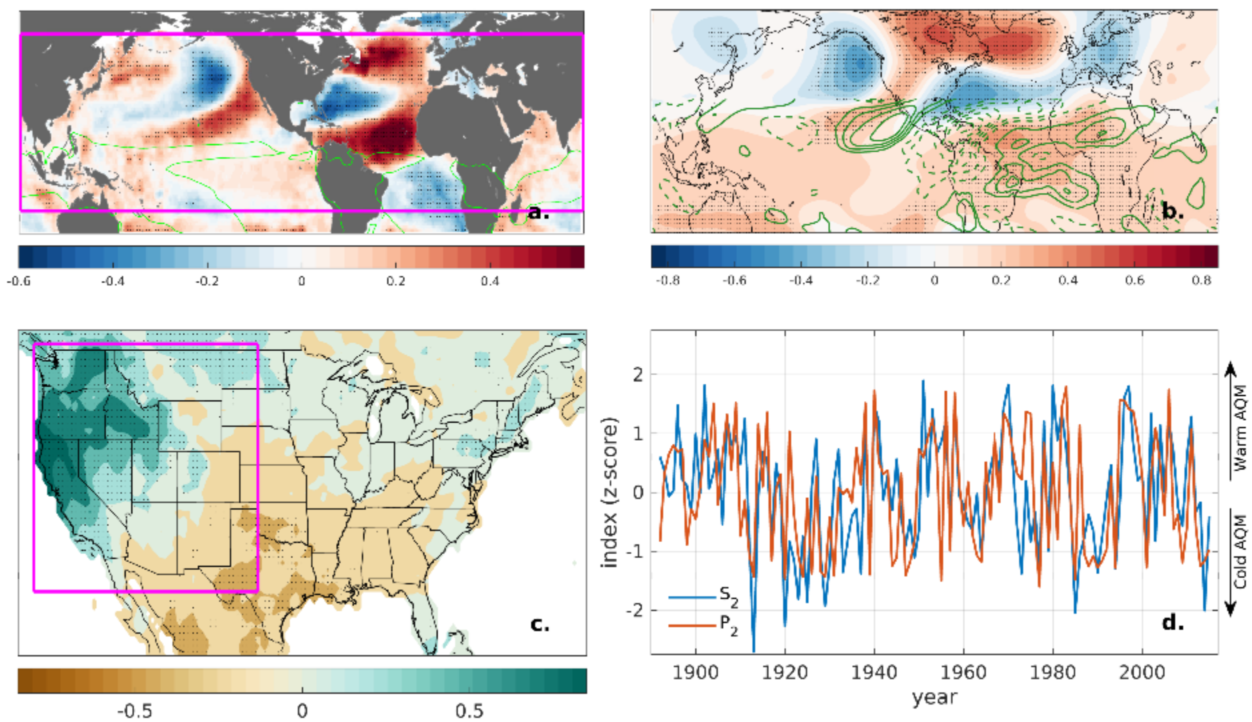

Figure 2.2. Same as Figure 2.1, but for the second mode of coupled variability (MCA2) between Atlantic sea surface temperatures and western US precipitation referred to as the Atlantic Quadpole Mode (AQM). The indices in the lower right panel show how the AQM evolved over time during the historical record, with positive values of the indices corresponding to the Warm Quadpole and negative values corresponding to the Cold Quadpole. In the Warm Quadpole, the anomalies of sea surface temperature and precipitation closely resemble the patterns mapped at left. In the Cold Quadpole, the anomalies of sea surface temperature and precipitation are the reverse of those mapped at left.

The cross-equatorial tropical Atlantic SST dipole associated with MCA2 flanks the region of high precipitation associated with the Intertropical Convergence Zone (ITCZ; green contour, Figure 2.2a). Positive *S2* tends to shift storminess northwest toward Central America (i.e., in Figure 2.2b, dashed contours over Central America and northern South America indicate enhanced storminess flanked by solid contours indicating diminished storminess). This shift appears to be associated with a teleconnection to the Gulf of Alaska trough (Figure 2.2b), which is responsible for the positive precipitation anomalies over much of the western U.S. We conducted more than 40 global climate model (GCM) experiments, each with 30 members, to test the causal mechanisms associated with the AQM, and results show some support for this tropical ITCZ mechanism (Stone, 2022). However, more GCM work is needed to investigate the mechanism further and to assess how well it is captured by seasonal forecast systems in operational use.

2.2 Interaction between ENSO and the Atlantic Quadpole Mode

Grouping precipitation patterns by phases of ENSO and AQM shows the familiar wet-north/dry-south pattern of La Niño years, and the familiar wet-south/dry-north pattern of El Niño years (Figure 2.3). These ENSO patterns provide little predictability in the transition zone between the anomalously wet and dry regions. In contrast, the AQM patterns shown in the lower row of Figure 2.3 depart from the traditional ENSO dipole pattern and provide information in the transition zone, with the Warm AQM corresponding to anomalously wet conditions and the Cold AQM corresponding to anomalously dry conditions.

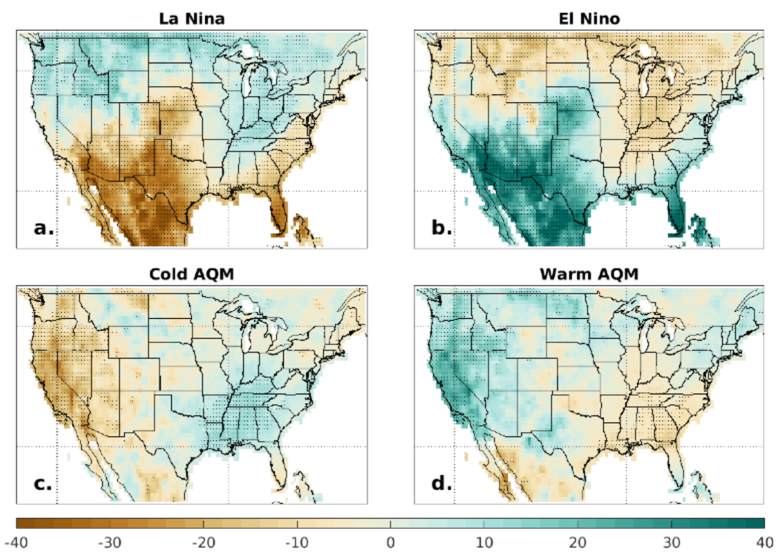

Figure 2.3. Observed December-March precipitation anomalies for La Niña years, El Niño years, Cold Atlantic Quadpole Mode (AQM) years, and Warm AQM years. Values are shown as percent anomalies.

Further separating western U.S. precipitation patterns to consider various combinations of ENSO and the AQM (Figure 2.4) reveals some important interactions between the two modes in which the AQM alters the alignment or strength of the seasonal precipitation impacts of ENSO. First, we note that the precipitation anomalies traditionally associated with ENSO appear most clearly under Neutral AQM (Figures. 2.4b,h). The Warm AQM is associated with above-average precipitation across most of the Intermountain U.S. (Figure 2.4, right column), whereas Cold AQM is generally anomalously dry over the western U.S. (Figure 2.4, left column).

During El Niño, Warm AQM shifts the zero precipitation anomaly transition zone north (Figure 2.4c), and Cold AQM shifts it south (Figure 2.4a). Previously ambiguous precipitation anomalies in the transition zone extending west to east from northern California through northern Colorado, become drier (wetter) during the cold (warm) AQM. Similarly, during La Niña, the warm phase of the AQM extends the transition zone farther south (Figure 2.4i), increasing the extent of the above-average precipitation anomaly.

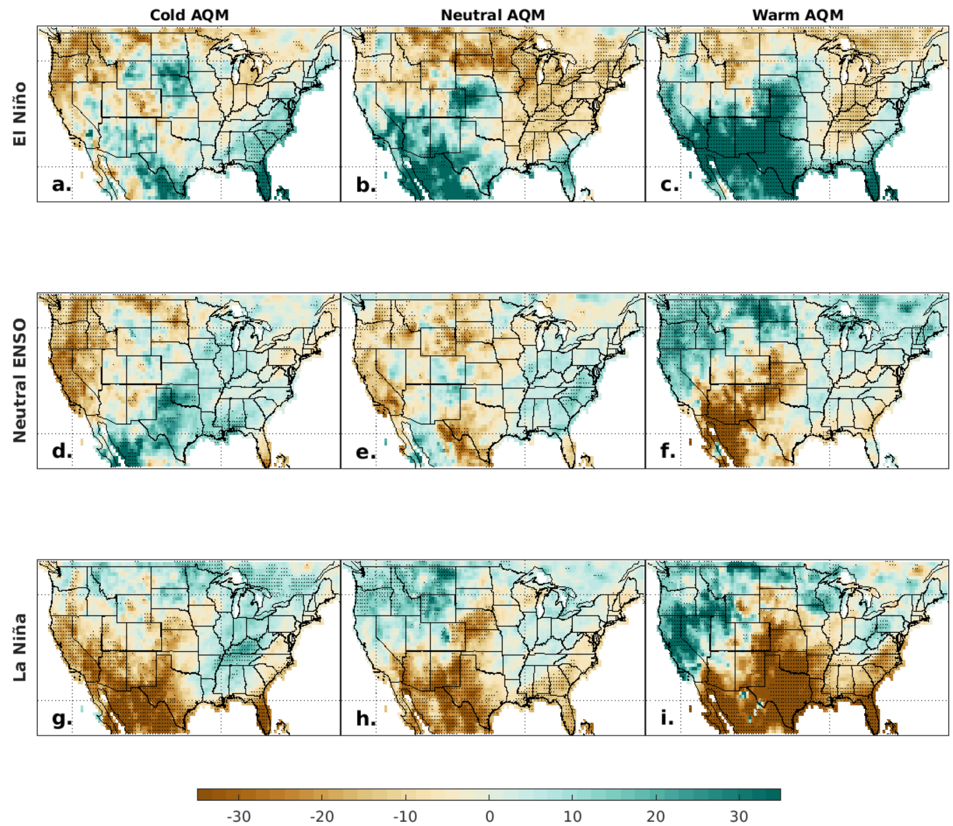

Figure 2.4. Observed December-March precipitation anomalies for various combinations of the Atlantic Quadpole Mode (AQM; columns) and El Niño-Southern Oscillation (rows). Values are shown as percent anomalies.

To complement the observational results and provide a much larger sample size for the coupled variability analysis, we analyzed a multi-millennial (10,000-year) present-day climate control simulation performed with a fully-coupled configuration of the Geophysical Fluid Dynamics Laboratory (GFDL) Climate Model (fully-coupled means the model has an atmosphere which interacts with the land, ocean, and ice models at the surface). Greenhouse gasses, ozone concentrations, and other external forcings were held constant at 1990 levels in this simulation to remove the confounding effects of climate change. Having approximately 1,000 winters in each of the ENSO-AQM combinations from the simulation yields results that are similar to but more smooth and statistically robust than the observed patterns (Figure 2.5). In composite precipitation anomalies for different combinations of MCA1 and MCA2 in the GFDL model (Figure 2.5), we see the familiar ENSO north/south precipitation dipole present in the neutral phase of the AQM (Figures 2.5b,h). During El Niño, as the AQM transitions from the Cold to Warm phase, the region of above-average precipitation expands north (Figures 2.5a-c). During La Niña, Warm AQM extends the above-average precipitation zone farther south, as seen moving from left to right in the lower row of Figure 2.5. For Neutral ENSO, Cold AQM is associated with a dry pattern over most of the Intermountain U.S. (Figure 2.5d) and Warm AQM is associated with the opposite (Figure 2.5f). Overall, the GFDL model precipitation anomaly patterns match the observations well, including the anomaly magnitudes and shifting of the transition regions as a function of the AQM phase.

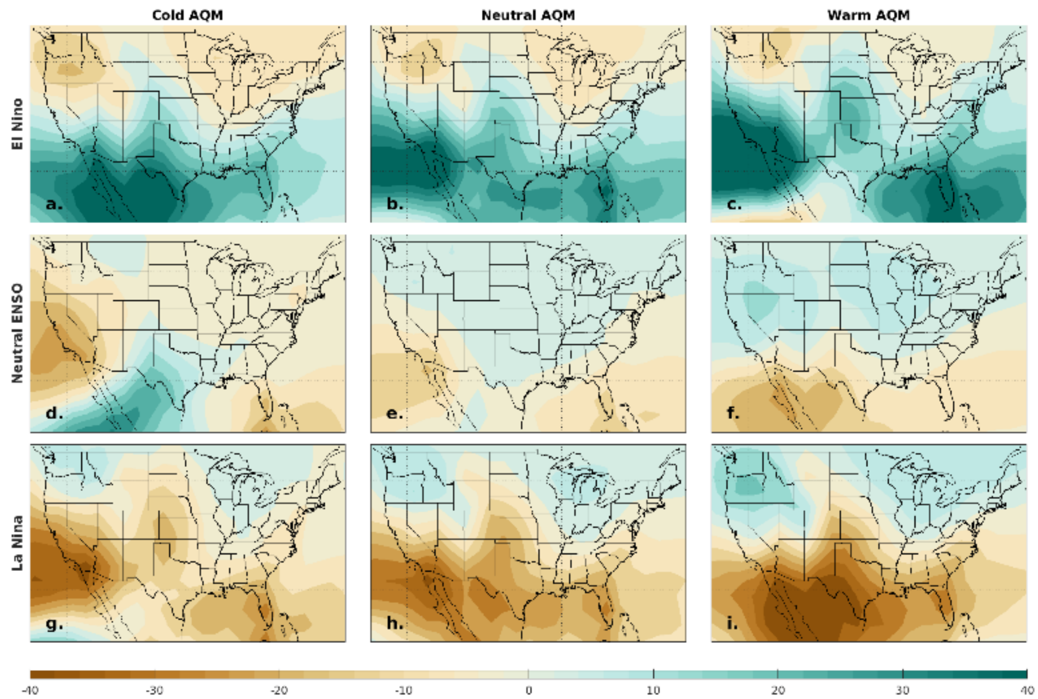

Figure 2.5. December-March precipitation anomalies as in Figure 2.4, but based on analysis of a 10,000-year global climate model simulation in which the confounding effects of climate change are eliminated by keeping greenhouse gas concentrations held constant at 1990 levels. The three columns correspond to the different phases of the Atlantic Quadpole Mode (AQM), and the three rows correspond to the three ENSO phases (El Niño, Neutral, La Niña).

2.3 Seasonal Planning Tools

Leveraging the scientific findings above regarding the AQM and ENSO, we developed a study region precipitation guidance tool (Figure 2.6). ENSO appears to exert important effects on study-region precipitation in conjunction with the AQM pattern. The values on the guidance tool indicate the winter precipitation percent anomaly expected for any combination of AQM and ENSO. Various indices of El Niño are readily available from the Climate Prediction Center (www.cpc.ncep.noaa.gov), and we are planning to work with web developers at Western Water Assessment to develop a convenient web-based portal for tracking the AQM index.

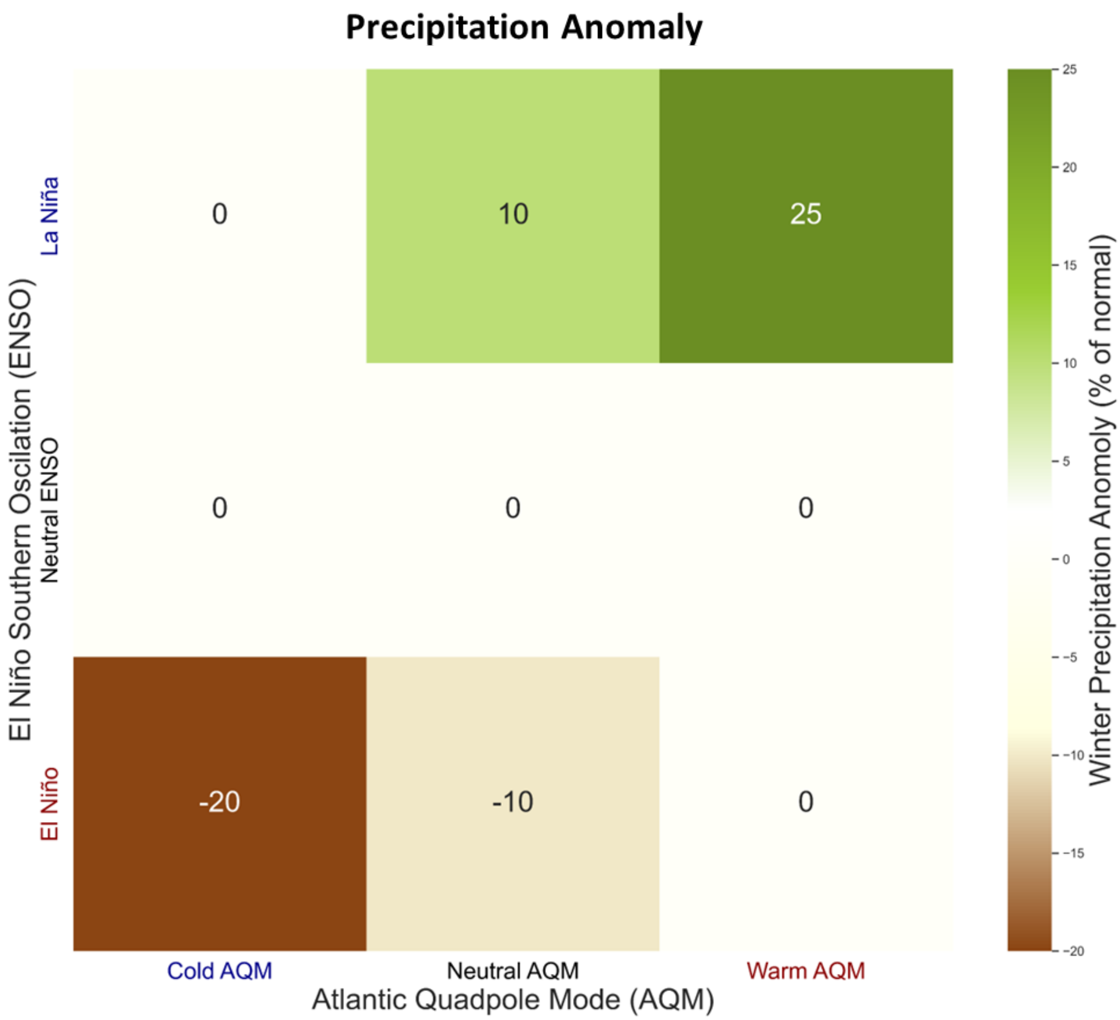

Figure 2.6. Percent anomalies of December-March study-region precipitation for different combinations of ENSO and the AQM.

The value of this research extends to water stakeholders outside the study region as well. To illustrate, the bar chart in Figure 2.7 shows the percent precipitation anomalies for each of the three watersheds in the transition zone where ENSO typically has minimal predictive value.

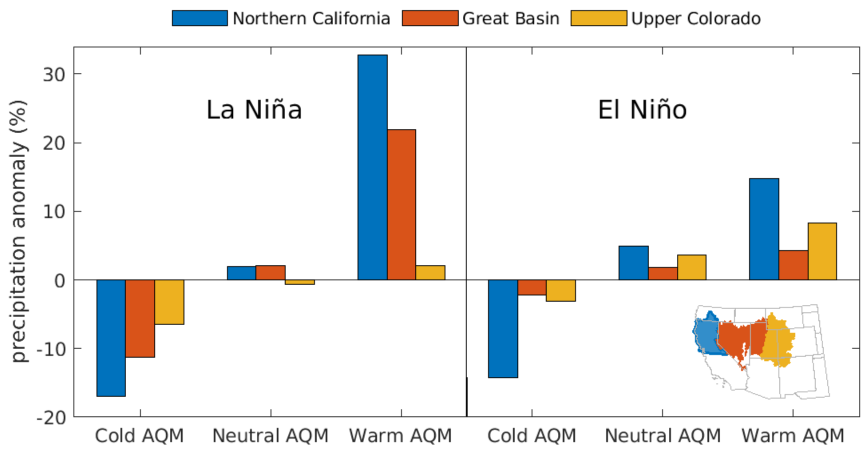

Figure 2.7. For three watersheds, percent anomalies of December-March precipitation corresponding to combinations of ENSO and AQM. The inset maps shows the three watershed boundaries, where the southern edge of Northern California (37.5°N) is near the latitude where ENSO precipitation anomalies become significant

3. Hydrology: Tool development and resolving key knowledge gaps identified during years 1-4.

Year 5 of our collaborative work with SLCDPU focused on integrating knowledge developed in years 1-4 of the project into useful tools to assist decision-making. This includes both coupled climate-streamflow-decision support models that integrate products from our three major research themes as well as stand-alone tools combining groundwater storage and precipitation that provide guidance on upcoming spring snowmelt in January. Our new research in Year 5 focused on two knowledge gaps underlying our statistical model of streamflow. Specifically, we used tritium (^3H) as an age tracer of groundwater to confirm or refute the presence of long-residence time groundwaters. We also began to evaluate the potential for mid-winter and spring vapor losses from the snowpack inferred from the finding that faster melt is positively related to both spring streamflow and groundwater recharge. We continued to publish and present our work in peer-reviewed literature and regional, national, and international meetings, effectively transferring the impacts of this project beyond SLCDPU.

Key Tools:

- Our major addition to decision support this year includes translating model results relating catchment-wide precipitation from PRISM and groundwater storage into "lookup tables" using SNOTEL SWE and January baseflow to predict spring runoff for each of the major supply catchments.
- We developed a multiple linear regression model to predict how groundwater storage, and by extension runoff efficiency, can be expected to change in response to future climate scenarios.

Key Discoveries:

- Our previous work that describes “quasi-decadal” periodicity in groundwater storage is actually composed of two patterns including a 3-4 year cycle since 1902 and a ~12-year cycle since 1955.
- Apparent groundwater ages range from 4 to 20 years in SLCDPU catchments, similar to the range observed in western headwater catchments throughout western North America.
- In the Great Basin, including SLCDPU supply catchments, there is an inverse relationship between apparent groundwater age and runoff efficiency.
- Slower and earlier snowmelt is likely to increase vapor losses from the snowpack, reducing runoff and groundwater recharge.

3.1 Predictive streamflow lookup tables

We have distilled the key findings underlying the interaction between current year precipitation and groundwater storage, controlled by multiple years of precipitation, temperature, and melt dynamics into “lookup tables” for each of the four major water supply catchments (Table 3.1). Each table provides a projection of the coming year's streamflow in acre-feet using predicted snow water equivalent (SWE) data from local SNOTEL sites and current (January) streamflow. January streamflow data is current while projected SWE data can be obtained from a range of sources including those provided by our climate modeling above or from the Climate Prediction Center.

Each cell in Table 3.1 represents a range of annual streamflow values given projected SWE and January streamflow. More precise estimates can be made using the full MLR models presented in previous reports.

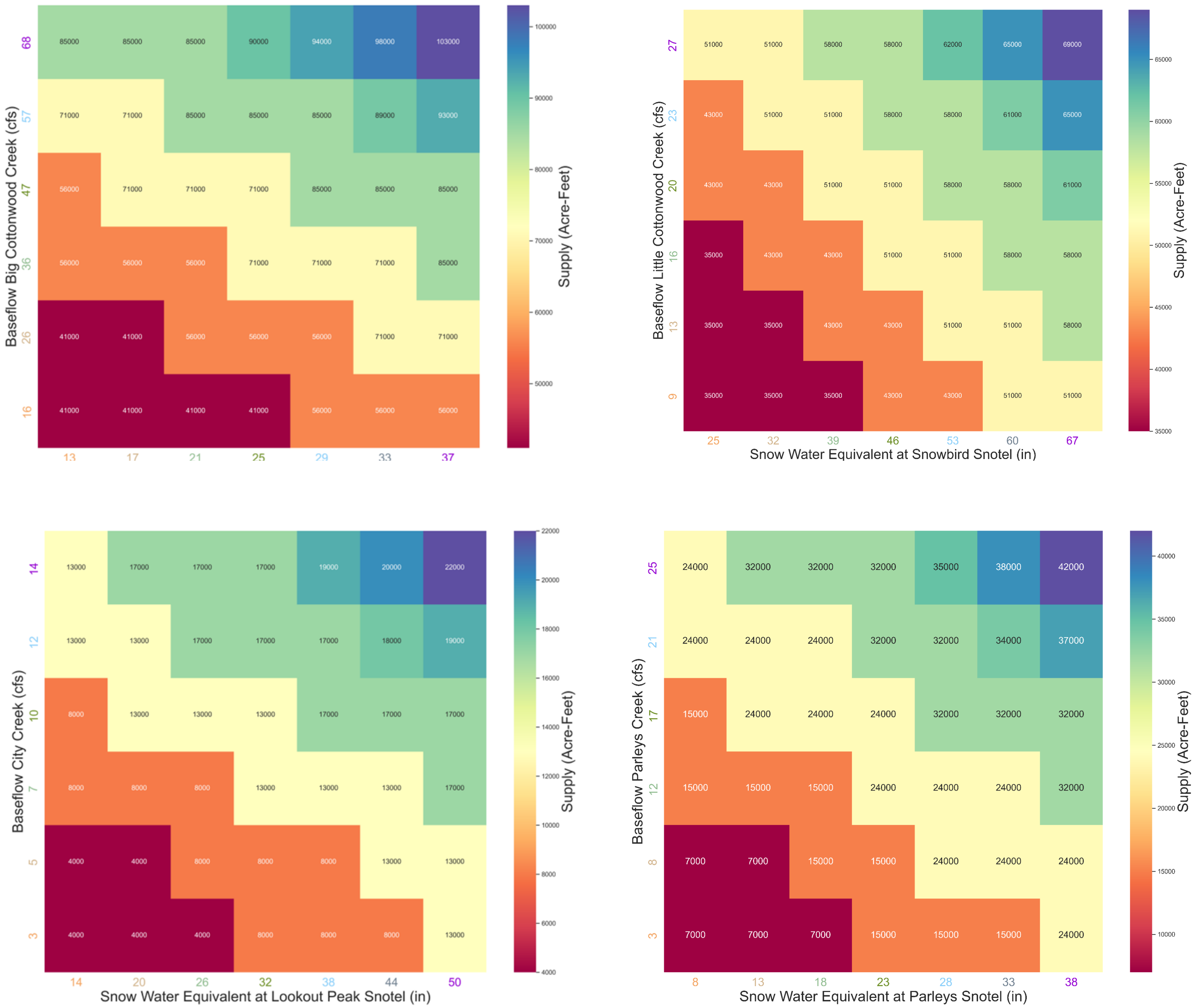

Table 3.1 Lookup tables for Big Cottonwood, Little Cottonwood, City Creek, and Parleys Creek provide estimated annual streamflow in acre-feet using observed January streamflow and predicted annual SWE at local SNOTEL stations. Full size tables can be found in Appendix A.3

Surface water supplies from the 4 major water-producing catchments in SLC (City Creek J CC, Parleys Creek J PC, Big Cottonwood Creek J BC, and Little Cottonwood Creek J LC) can vary between 30,000 acre-ft/year to 200,000 acre-ft/year. As we would expect, wet years often lead to higher runoff than dry years, however, runoff efficiency (the fraction of precipitation that makes it to streamflow) can still be lower than expected even if the Wasatch mountains receive above-average precipitation.

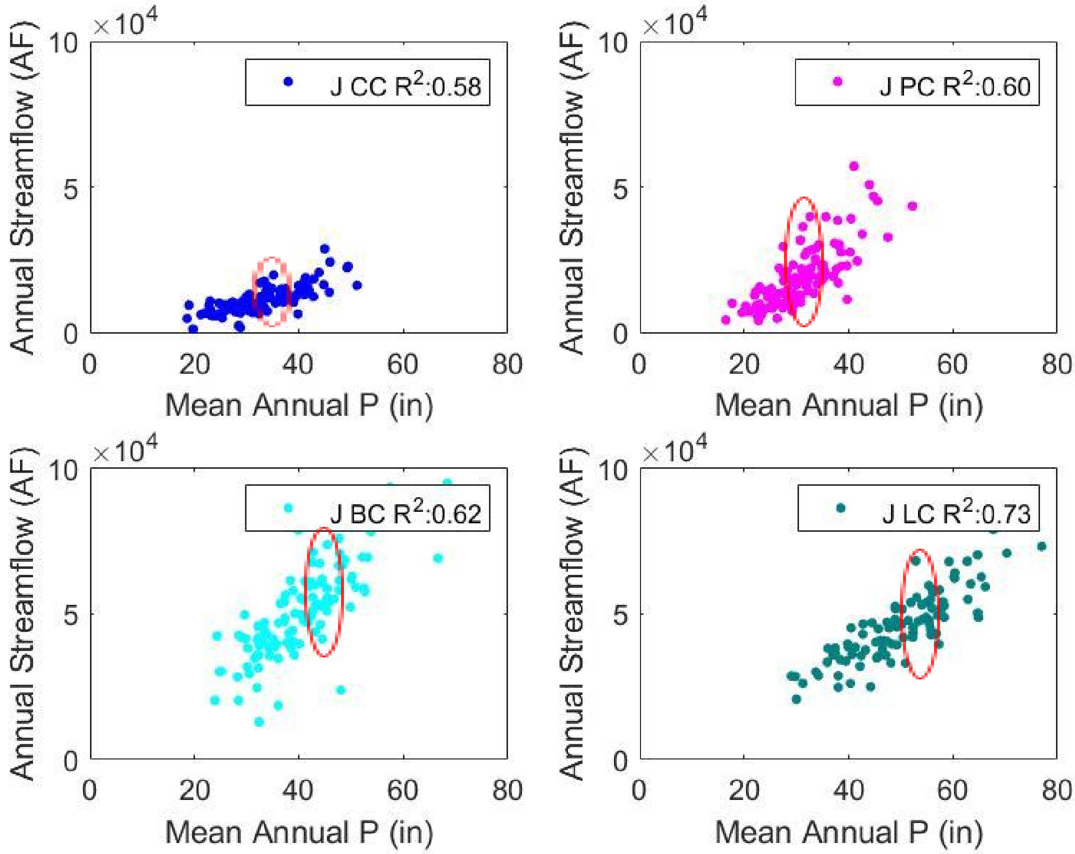

Figure 3.1 Mean annual catchment precipitation (in/year) compared to annual streamflow (acre/ft/year) in City Creek (J CC), Parleys Creek (J PC), Big Cottonwood Creek (J BC) and Little Cottonwood Creek (J LC). Precipitation alone explains approximately half of the variability in streamflow (r^2 = 0.56). Red circles indicate the range of expected streamflow for each water supply catchment given average mountain precipitation.

As seen in the lookup tables (Table 3.1), including antecedent catchment conditions represented through winter baseflow further reduces the uncertainty observed in annual runoff.

3.2 Multiple Linear Regression Model of groundwater recharge

To assess the drivers of recharge under current and potential future climate scenarios, we return to our analyses of ten regional catchments that include both warmer and drier conditions than those observed in SLCDPU water supply catchments. Across this broader range of sites, MLR models demonstrated that annual variability in groundwater recharge, inferred from January streamflow, was significantly related to a number of antecedent climate variables over the previous four years ($p<0.05$) (Figure 3.2; Table 3.2). The periodic variability in winter baseflow was significantly related to the concurring water year's fall precipitation (9/10 catchments), 1-4 years of antecedent precipitation (all catchments), 1-3 years of previous melt rate and/or duration (9/10 catchments), and 1 year of antecedent temperature (8/10 catchments). The number of variables retained as significant in each regression ranged from as few as two in Little Cottonwood Canyon (J LC) to as many as 10 in City Creek (J CC). The strongest predictors of change in storage / January baseflow in all catchments were the concurring year's fall precipitation (β= 0.14-0.56)(Table 3.2), the previous year's annual precipitation (β= 0.14-0.57)(Tbale 3.2), or the previous year's melt rate (β= 0.07-0.44)(Table 3.2. Here, the β values are regression coefficients for predictors scaled to have mean of zero and variance of 1, so their values indicate the relative strength of the statistical relationship.

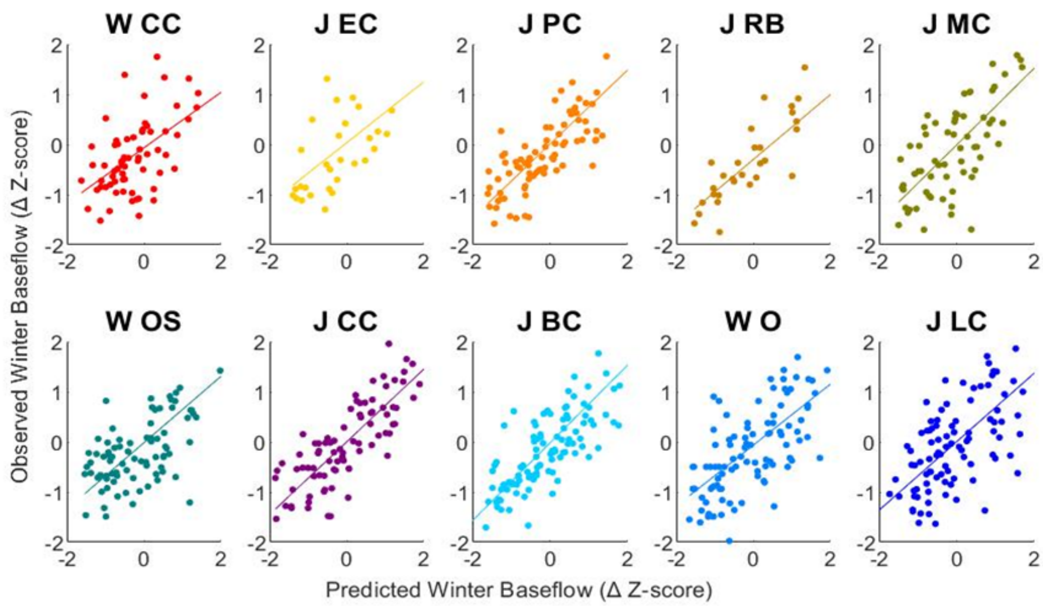

Figure 3.2: Predicted winter baseflow using antecedent precipitation, temperature, melt rate and melt duration, compared to observed winter baseflow in ten regional catchments, seven in the Jordan River Basin including Emigration Creek (J EC) Parleys Creek (J PC), Red Butte Creek (J RB), City Creek (J CC), Big Cottonwood Creek (J BC), and Little Cottonwood Creek (J LC) and three in the Weber River Basin including Chalk Creek (W CC), Weber at Oakley (W O),a nd Ogden South Fork (W OS). Because predictor values of precipitation, temperature, and melt vary dramatically, all values are normalized using z-scores with means of 0 and variance of 1 allowing direct comparison between catchments. On average, the model better predicted winter baseflow in warmer and drier (lower runoff efficiency) catchments (r^2>0.7).

The MLR models better predicted recharge / January baseflow in warmer and drier catchments, ($r^2 > 0.7$ for W CC, J PC, J RB, J MC) than in cooler and wetter catchments ($0.70 > r^2 > 0.46$ for W OS, J CC, J BC, W O, and J LC) (Table 3.2). J EC was an exception to this overall pattern. Although J EC is relatively warm and dry with a low water yield or runoff efficiency (RE = 0.18), predictability was low ($r^2 = 0.29$) compared to catchments with similar climate regimes.

Catchments	Precipitation					Temperature		Normalized Melt Rate			Normalized Melt Duration			
	wy(Fall)	wy-1	wy-2	wy-3	wy-4	wy-1	wy-4	wy-1	wy-2	wy-3	wy-2	wy-3	Y-int	R^2
(W CC)	+(0.38)	+(0.57)	+(0.24)	+(0.11)	+(0.17)	-(0.24)		+(0.07)	-(0.07)				(0.03)	**0.84**
(J EC)		+(0.14)				-(0.06)		+(0.44)	+(0.02)				(0.06)	**0.29**
(J PC)	+(0.40)	+(0.38)	+(0.23)			-(0.08)	-(0.07)	+(0.12)	+(0.08)				(-0.01)	**0.62**
(J RB)	+(0.28)	+(0.41)	+(0.27)	+(0.09)		-(0.22)		+(0.11)				+(0.18)	(-0.11)	**0.87**
(J MC)	+(0.12)	+(0.39)	+(0.19)		+(0.06)	-(0.14)		+(0.17)	+(0.19)	+(0.06)			(-0.04)	**0.70**
(W OS)	+(0.49)	+(0.41)				-(0.09)		+(0.04)					(0.02)	**0.46**
(J CC)	+(0.14)	+(0.40)	+(0.19)			-(0.24)	-(0.09)	+(0.26)	+(0.03)	+(0.08)	+(0.09)	+(0.15)	(0.04)	**0.67**
(J BC)	+(0.38)	+(0.35)	+(0.13)		+(0.1)	+(0.08)		+(0.21)	+(0.04)				(-0.07)	**0.58**
(W O)	+(0.30)	+(0.47)	+(0.23)	+(0.13)	+ (0.17)			+(0.15)	+(0.06)				(-0.01)	**0.61**
(J LC)	+(0.56)	+(0.36)											(0.01)	**0.47**

Table 3.2: Antecedent meteorological variables included in MLR model to predict winter baseflow. MLR equation: *Δ Winter baseflow= β Precipitation$_{(n-i)}$ + β Temperature$_{(n-i)}$ + β Melt Rate$_{(n-i)}$ + β Melt Duration$_{(n-i)}$* . Here, *wy* denotes current water year, *i* is the number of years in the past (eg. *n-1* indicates 1 year previous), the *β* terms are regression coefficients, R^2 is the fraction of observed variance explained by the model, and bold indicates statistical significance (*p*-value less than 0.005).

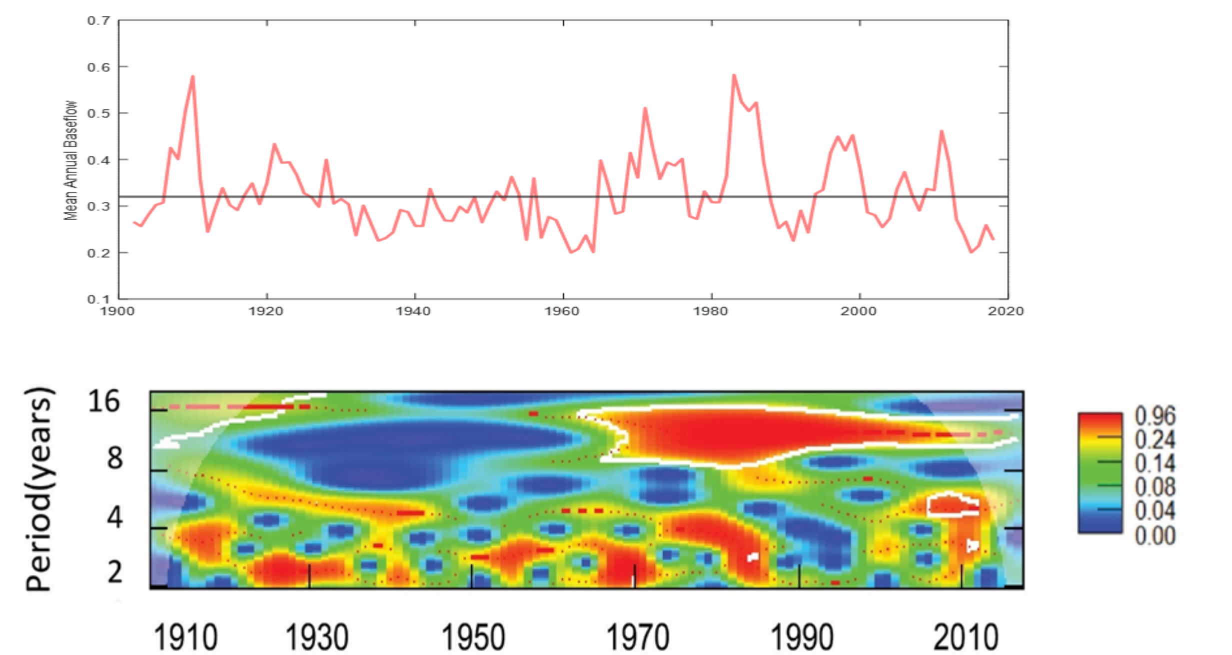

Figure 3.3. Top panel shoes mean winter baseflow annual vairbailty in the last century. Bottom panel shows wavelet transform analysis of mean winter baseflow across all catchments. Winter baseflow provides an index of groundwater storage with warmer colors indicating that groundwater storage across all of northern Utah exhibits coherent, cyclical patterns in space and time. Specifically, groundwater storage exhibits 3-year periodicity of high correlation/power level (0.23) (red values) over the full 100 year record and a late-century significant periodicity (white outline) power level (0.29) at a ~12-year periodicity.

3.4 Groundwater ages and runoff efficiency

We obtained external support from the National Science Foundation (NSF) to sample age tracers (^3H) in winter baseflow and spring snowmelt samples throughout the west. Included in the project are multiple samples collected from SLCDPU water supply catchments and other regional headwater catchments (Figure 3.4). Apparent groundwater ages range from 4 to 20 years in SLCDPU catchments, similar to the range observed in western headwater catchments throughout western North America. The inverse relationship observed in the blue dots in figure 3.4, suggests that in higher efficiency catchments, where a larger fraction of precipitation makes it to streamflow, apparent age is younger than in lower runoff efficiency catchments. The coherence between older ^3H ages and statistical sensitivity to more years of antecedent climate in our models increases confidence that our lookup tables are capturing physical processes and not spurious correlations.

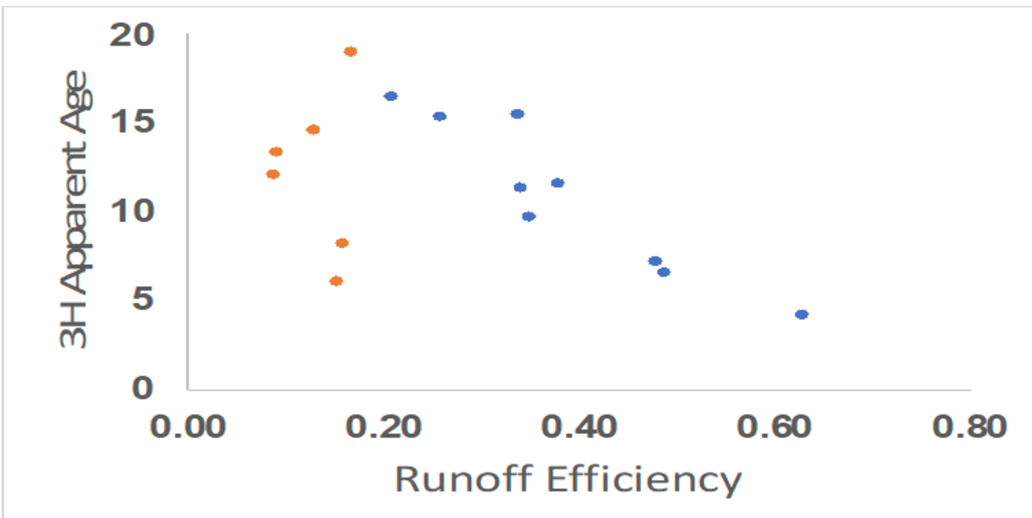

Figure 3.4: In the Great Basin, including SLCDPU supply catchments, there is an inverse relationship between apparent groundwater age and runoff efficiency (RE) for locations with 0>.20 RE (Blue dots). Below an RE of 0.20 ages is much more variable.

3.5 Initial analyses of snowpack vapor losses

Using leveraged funding, we have developed preliminary data addressing the potential for warmer (e.g. higher energy) snowpacks to lose water through either evaporation or sublimation. We briefly highlight initial results here which suggest that up to 40% of the snowpack may be lost in higher-energy environments (Figure 3.5). This suggests that slower and earlier snowmelt reduces both runoff and recharge by increasing vapor losses from the snowpack during winter and spring.

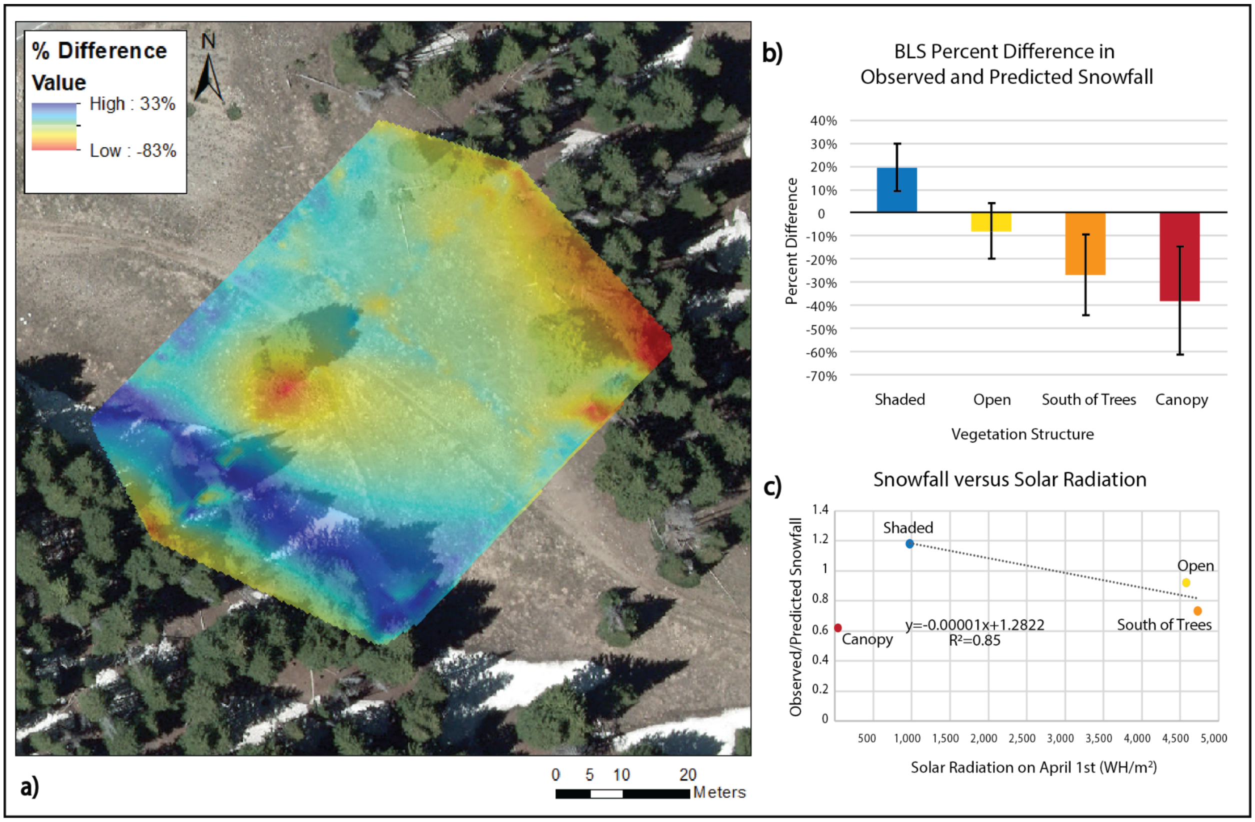

Figure 3.5. High spatial resolution snow surveys in Big Cottonwood Canyon document that up to 40% of annual snowfall (spatially averaged) can be lost to vapor flux before melt begins. These losses occur in high-energy environments (warmer) that serve as proxies for snowpack ablation during years with earlier and slower melt.

4. Engineering: Developing tools and integrating system modeling methods to enhance operational water management

Previous research activities advanced the understanding of the climate, population growth, and operational factors influencing the reliability, resilience, and vulnerability (RRV) of the water system. We integrated the potential infrastructure and operations highlighted in the *Supply and Demand Master Plan* into the Salt Lake City Water Systems Model (SLC-WSM), including but not limited to new source development, water reuse, and increasing the preferred volume of storage in the MWDSLS system. Using the SLC-WSM, our research evaluated the performance of the water system to historically observed variability and, driven by advancements in the understanding of the governing climate-hydrology interactions (i.e., single to multi-year flows related to climate signals), the projected response of streamflow to climate change. Using the volume of water requested from Deer Creek reservoir as a metric to gauge the performance of the water system (i.e., due to additional treatment, transfer, and pumping costs), model simulations indicated large accuracy improvements by integrating climate-sensitive estimates of demand. The comprehensive assessment of the water system leveraging hydroclimate-driven supply and demand influences on performance supports refined estimates of the timing, magnitude, and duration of supply requests from Deer Creek reservoir. The use of the

Climate-Supply-Development Water Demand Model (CSD-WDM) supported the effort to characterize seasonal estimates of demand in response to variations in annual hydroclimate anomalies but needed an improved end-user interface for operations.

Building on the climate-supply theme, we performed a trend analysis to characterize the timing, duration, and intensity of hydrological drought in the region, and by proxy, the variability and magnitude of historical deficits (i.e., volume of surface water supply below the historical average). Evaluating the trends in the SLC-WSM highlighted the performance of the water system exhibiting greater sensitivity to mild multi-year droughts compared to extreme single-year drought events. While downscaled GCM-driven projections of streamflow provide useful insights into the anticipated impacts of climate change, there is a need to assess the performance of the water system based on the probability of available supply.

Studies have looked at the severity, duration, and frequencies of droughts based on different drought indices, but no guidelines exist on using univariate and multivariate frequency analysis in an operational way. The drought severity-duration-frequency (SDF) information on droughts has not yet been standardized like the flood frequency analysis in the Bulletin 17C or the rainfall depth-duration-frequency (IDF) curves available from the National Weather Services (NWS) of the National Oceanic and Atmospheric Administration (NOAA).

The lack of a standard guideline is important to address because water utilities must develop adaptation plans including new water infrastructure, demand management, and exploring non-conventional water sources. The adaptation and mitigation plans must be based on evidence that can provide frequency as well as time domain information to the water utility about the risks from a range of streamflow deficit events. This study advanced the use of a technique called the retro-prospective technique, enabling water managers to develop a streamflow time series representing streamflow deficit events from the empirically developed SDF curves representing the complete spectrum of severity and duration of deficits in the historical streamflow record.

The Engineering work for Year 5 leverages our cumulative years of advancements in the understanding of the Salt Lake City water system to develop water system management products that enhance the operational capacities of the utility. The research advancement led to two operational tools: 1) hydroclimate-driven demand estimator and corresponding water system performance index tables built off a comprehensive set of water system simulations to variations in hydroclimate (i.e., air temperature, precipitation, snowpack, streamflow) and 2) SDF curves and complementary tables and charts for multi-year streamflow deficit scenarios of specific return periods showing the expected volume and the deficit in the volume of water relative to average volume in a given year.

The demand modeling work leveraging the CSD-WDM illustrates the connectivity between the total water demand of the Salt Lake City system to variations in hydroclimate (i.e., variations in mean monthly air temperature and cumulative monthly precipitation). Additional research into the hydroclimate connection to demand indicates that the conditions observed in April and May exhibit a strong relationship to outdoor water use spanning June to October. The findings and corresponding research tools support the assessment of the compounding influences of climate on supply, demand, and the overall performance of the water system - likely mirroring the Atlantic Quadpole Mode and hydrological base flow signals demonstrated by the Climate and Hydrology teams (Sections 2 and 3).

The engineering research activities bring together the state-of-the-science from the Climate, Hydrology, and Engineering teams into actionable and informed operational tools for SLCDPU. The engineering team produced the following key discoveries and tools as part of the Year-5 scope of work.

Year-5 key discoveries/tools:

- We identified a practical-knowledge gap surrounding the lack of usable multi-year streamflow deficit information for water supply planning and management. Addressing the research and operational need, we applied a univariate frequency analysis of the historical streamflow deficit for multiple years to support a supply event-based planning and management strategy for the SLC water system.
- For this study, we addressed the SLCDPU need for SDF curves and we derived the corresponding streamflow analogs and deficits. We built on previously provided SDF curves and accompanying tables for the standard return intervals (10-yr, 50-yr, and 100-yr) and the deficit in streamflow volume for each creek on an annual basis - a matrix of negative volumes.
- Hydroclimate conditions during April and May strongly influence seasonal water use, with the mean daily temperature of April and May identified as key indicators of April through October water use and generally exhibiting a positive feedback, i.e., an increase in temperature results in an increase in per-capita outdoor water use.
- Leveraging advancements in machine learning, we developed a demand simulation tool to build a lookup table of seasonal estimates of water demand based on percent changes in temperature and precipitation (i.e., hydroclimate).
- We developed lookup tables displaying the estimated volume of out-of-district Deer Creek water required to prevent system deficits for a range of surface water supply (i.e., from climate and hydrology groups) and demand scenarios (i.e., produced by lookup table from the engineering group) to support proactive water system management (e.g., demand hedging).

We break down the summary of results and deliverables below, with the objective of defining the overall theme of each section and subdividing it by the sub-tasks.

4.1 Develop a workflow to use SDF curves for analysis of multi-year low-flow scenarios

The Engineering team completed the analysis of historical hydrological trends and accomplished the development of SDF curves for the surface water supply sources of SLC. Building upon the accomplishments from Year 4, we operationalized the SDF curves for use in multi-year water supply system impact analysis and decision-making. Below are the results of the three subtasks connecting SDF curves to operations.

4.1.1 Probabilistic Supply Estimator within the SLCDPU timeline and planning horizon

The operationalization of the developed SDF curves is achieved by introducing a concept called the retro-prospective approach, which in simple terms means looking back in the past to estimate the possible conditions in the future. Based on this concept and collaborations between the utility and research groups, the closure of the water year was identified to be the optimal time for the use of the SDF curves. Given the tool leverages the relationships between interannual surface water supply yields (i.e., percent surplus or deficit of the historical average relationship to the next few years), the timing of application in October (i.e., the start of the new water year and completion of the prior) complements the tools from the other teams. Specifically, it aligns with the anticipated precipitation anomaly provided by the climate team and establishes a range of streamflows for the following year based on the relationship between the present conditions and historical frequency. We developed the Probabilistic Supply Estimator to serve as both the first approximation of surface supply yield for the following year and to function as a long-term planning tool for applying an acceptable level of risk to decision-making, complementing the Hydrology team's annual supply estimates beginning in February. The long-term planning tools build on the probabilistic capabilities identified in the SDF analysis, e.g., what is the probability of experiencing below-average supplies for the next three years? The Probabilistic Supply Estimator supports risk-tolerance-based decision-making for estimates of surface water yields with an event horizon extending to five years. The SDF curves for 2-5 years durations for the Big Cottonwood Creek are shown below in Figure 4-1. From the SDF curves, any selected point corresponds to a streamflow time series in the historical record of streamflow data. Thus, a streamflow time series for any point can be derived by matching the level of severity and duration of the event selected.

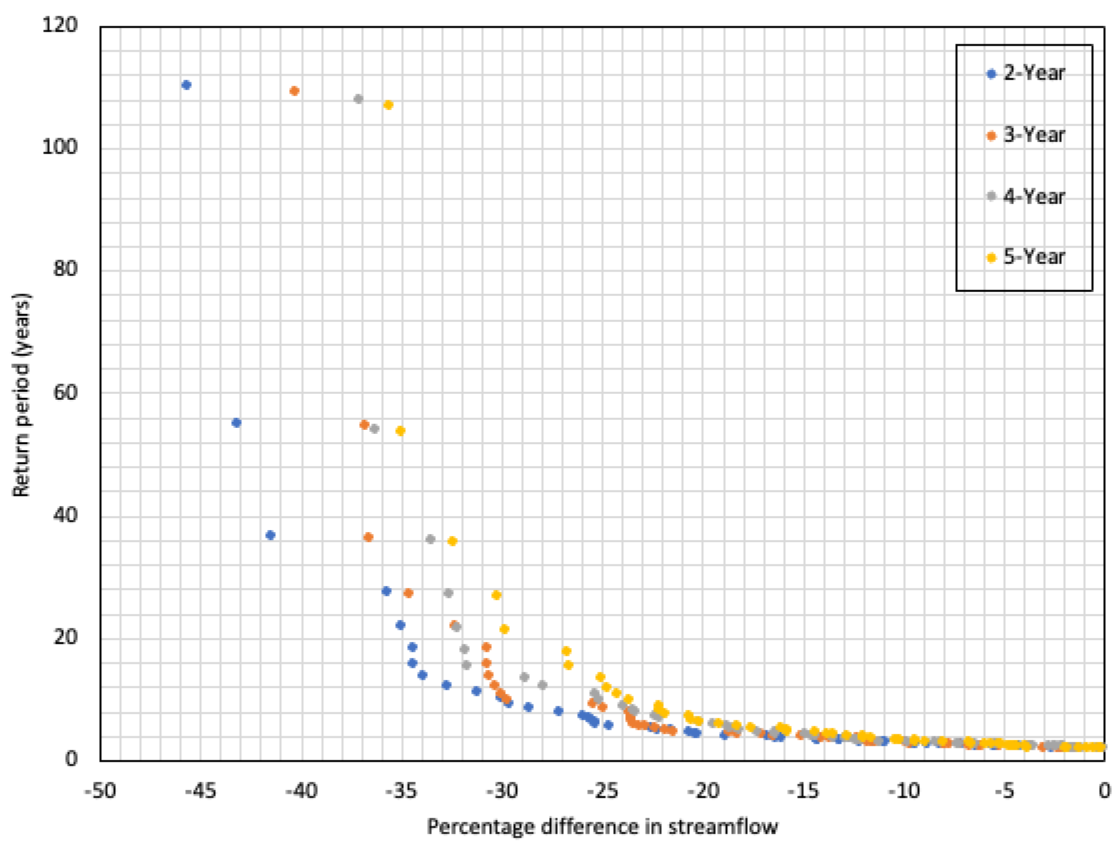

Figure 4.1. Multi-year streamflow deficit SDF curves for Big Cottonwood Creek

4.1.2 Operationalizing the SDF curves

While lookup tables provide easy-to-reference estimates of streamflow, we recognize that the utility may want to use hydrographs at a daily resolution of the water year for their own water system analysis. From Figure 4.1 above, the most severe 2-year streamflow deficit in the plot, i.e., a return period of 110 years, has a severity of 45%. A streamflow time series corresponding to this deficit is provided below in Figure 4.2.

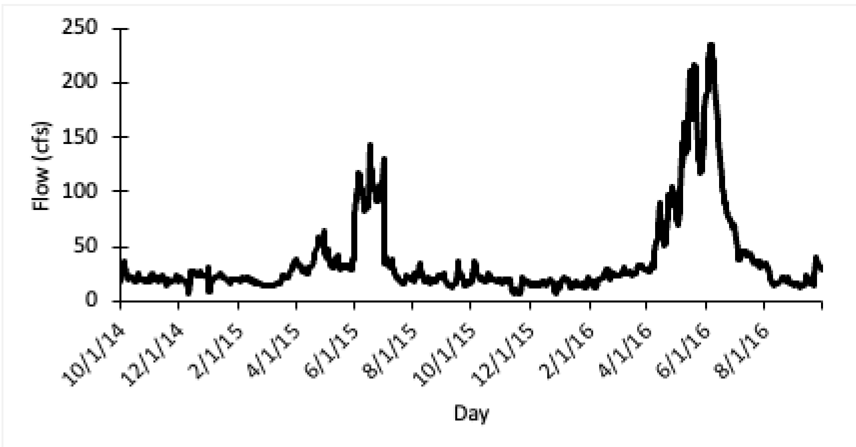

Figure 4.2: Streamflow time series analog for the 110-yr return interval, 2-year duration streamflow deficit event for the BCC

As discussed in section 4.1.1, we developed a new technique called the retro-prospective approach, linking the historical streamflow information to the estimated streamflow in future years. We recommend applying the retro-prospective approach at the end of the water year where the utility can determine the recently completed water year deficit in relation to the historical mean, e.g., if the annual yield is below the mean yield, the previous water year is a deficit year. Next, the utility selects an event of interest (i.e., an event-based return period or periods of interest that will provide the severity of the deficit) from the streamflow deficit SDF curves for a respective planning horizon. The workflow provides a streamflow analog for the selected probability of the event determined by the SDF curves' respective severity and duration within the streamflow record. The streamflow time series can then support an event-based impact analysis of the water system.

4.1.3 Applying the SDF curves and Streamflow Analogs for System Impact Analysis and Informed Decision-Making.

The SDF curves and streamflow analogs provide a novel early-season water resources planning tool connecting a supply-sided probability of occurrence to the severity of a possible deficit. However, it is necessary to note that the term deficit here refers to below-average conditions for any selected period. For example, for 2 years, the deficit is calculated as below the 2-year moving average flow, and so on for other durations. Table 4.1 shows the streamflow deficits for standard return periods (10, 50, and 100 years) of 2-5 year durations.

Table 4.1: Multi-year streamflow deficit levels (in percentage below average) for 2-5 year duration of standard return periods for the three creeks of SLC.

Big Cottonwood Creek	**Duration (years) & Severity of Deficit (percentage)**			
Return Period (year)	2	3	4	5
10	**-30**	**-30**	**-25**	**-24**
50	**-42**	**-34**	**-35**	**-33**
100	**-45**	**-40**	**-37**	**-35**
Little Cottonwood Creek	2	3	4	5
10	**-26**	**-23**	**-21**	**-20**
50	**-36**	**-29**	**-28**	**-27**
100	**-40**	**-31**	**-30**	**-30**
City Creek	2	3	4	5
10	**-36**	**-33**	**-30**	**-27**
50	**-41**	**-40**	**-38**	**-36**
100	**-44**	**-43**	**-40**	**-39**

To eliminate the need to repeatedly use SDF curves and search for streamflow analogs for different events of streamflow deficits, we developed charts and tables to convert the streamflow analogs to the projected volume deficit in a given water year. For return periods of 10, 50, and 100 years and streamflow deficit duration of 2-5 years, the expected volume of water relative to the average volume for each creek is shown below in Figures 4.3, 4.4, and 4.5.

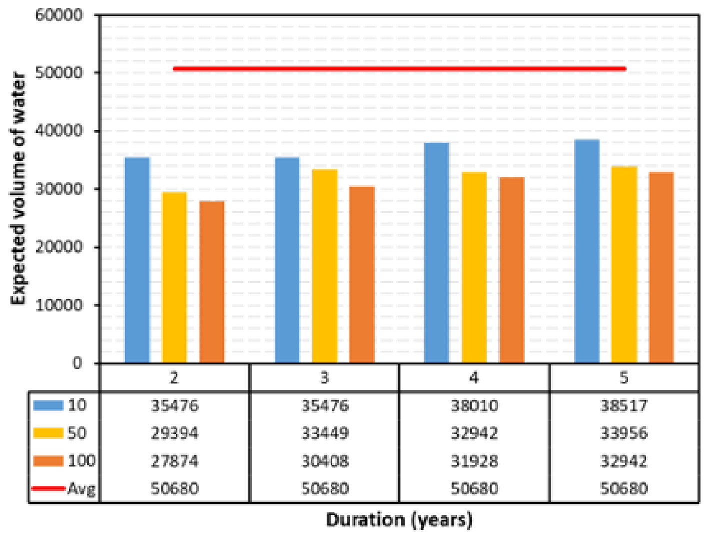

Figure 4.3. Expected volume relative to the average volume of water from the Big Cottonwood Creek for a given duration of streamflow deficit of standard return periods. Units are acre-feet.

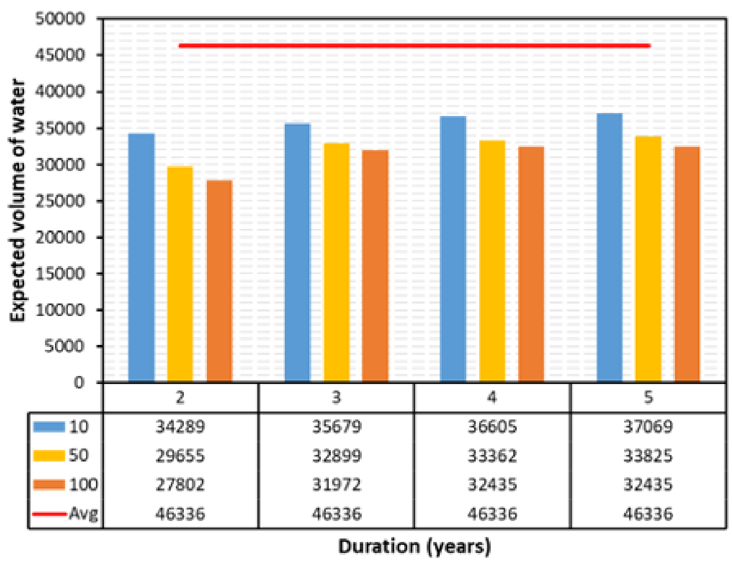

Figure 4.4. Expected volume relative to the average volume of water from Little Cottonwood Creek for a given duration of streamflow deficit of standard return periods. Units are acre-feet.

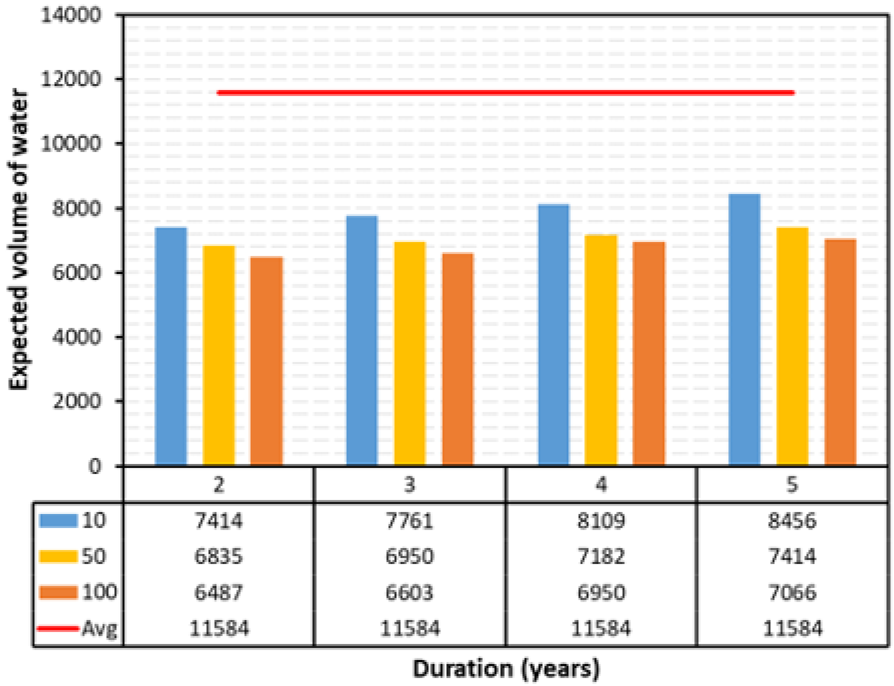

Figure 4.5. Expected volume relative to the average volume of water from City Creek for a given duration of streamflow deficit of standard return periods. Units are acre-feet.

The above three figures show the volume available in a given year for a given duration. For example from Figure 4.3, for a return period of 100-year (i.e., an event that has an exceedance probability of 1%), the annual water volume for the 5-year duration is ~33,000 acre-feet. Compared to the average, this is a deficit of 18,000 acre-feet in a given year.

In Figure 4.6 below, for a streamflow deficit duration of 5 years and a return period of 100 years, the total deficit (from the three creeks combined) on an annual scale is shown (i.e., 36,500 acre-feet). This is the amount of water shortage in the system if a streamflow deficit event of a 5-year duration of a 1% chance occurs. The 36,500 acre-feet of water is what is required to bridge the gap in demand and supply. Here, it is essential to mention that for these five years, the demand as well as supply from other sources is assumed to be constant. Thus, this deficit can be bridged by requesting 36,500 acre-feet of water each year from the Deer Creek reservoir. Additional requests from the Deer Creek system each year mean additional costs to the utility and also deplete the storage in the reservoir, thus increasing the vulnerability of the system.

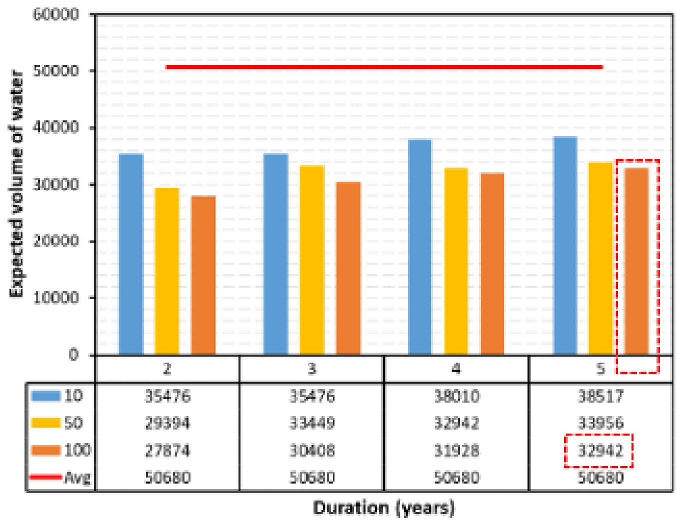

Annual deficit relative to average available water volume (acre-feet)

Big Cottonwood Creek	Little Cottonwood Creek	City Creek	Total
18000	14000	4500	36500

Figure 4.6. Demonstration of the calculation of the deficit in the system on an annual scale from all three creeks for any selected duration and return period. Only the expected volumes of Big Cottonwood Creek are shown on the left, and the table on the right shows the deficit for all three creeks.

4.2 Advance and apply Hydro-ML modeling to guide water system management operations to seasonal supply limiting conditions

Key Discovery 3. Mean air temperature and cumulative precipitation during April and May exhibit a strong influence on total seasonal water use and overall water system performance spanning April to October.

A primary focus of the Engineering team's effort during year 5 was to leverage advancements in Hydro-ML, integrate and couple with the existing SLC-WSM framework, and process the information in useful tools to enhance the management and operations of SLCDPU's water system. The goal of the research activities was to develop tailored water systems tools linking climate, streamflow, and demand projections to inform on seasonal water system performance without the need to run an array of stochastic simulations. Due to the multi-disciplinary connections in the development of the engineering tools, the tools are most useful when coordinated with the use of the climate and hydrological tools described in Sections 2 and 3. The research-to-operations workflow is an example of academic-practitioner interactions and has led to one accepted peer-reviewed article, three in-submission peer-reviewed articles, and several conference presentations. Descriptions of the research and tools are in the following subsections.

4.2.1 Operationalize Water Demand Prediction

The goals for operationalizing water demand prediction involved the exploration of a variety of advanced deep learning algorithms to 1) enhance the prediction of hydroclimate-urbanization-driven water demands and 2) develop the cyberinfrastructure to operationalize the model. The initial Climate-Supply-Development Water Demand Model (CSD-WDM) relies upon linear driver-demand statistical relationships (see Year 4 report for more information). From a modeling perspective, there is an opportunity to integrate modeling methods capable of capturing nonlinear driver-target interactions that have the potential to improve the predictive performance of the water demand model, notably during April, May, and October. Complementing algorithm development, the engineering team established the framework to bring the CSD-WDM from research into operations. Research activities under this scope of work integrate the measurement of uncertainty into the forecast and the development of lookup tables to support annual total production demand estimation.

We explored Multilayer Perceptron (MLP) neural networks and Random Forest Regression (RFR) tree-based machine learning (ML) algorithms to evaluate model complexity vs. accuracy to the existing ordinary least squares (OLS) algorithm. We selected the MLP model for its demonstrated performance throughout many applications in water resources modeling and built the MLP network with the support of the Keras package within Tensorflow v2.4.1 and the drivers of demand identified by recursive feature elimination (RFE) from the OLS algorithm. The MLP network consists of an input layer that receives the predictors, middle hidden layers with nodes/neurons that form the computational engine, and an output layer that produces the prediction. Model training consisted of the following parameters: rectified linear activation function (ReLU), two to eight hidden layers with neurons ranging from 8 to 128, the Adam optimizer, and 500 epochs. During training, we use five-fold cross-validation with backpropagation gradient descent to weight the network and minimize error (i.e., Root Mean Square Error, *RMSE*). We selected the RFR algorithm for its demonstrated high proficiency in transforming data into estimates of demand without relying on rule-based programming for applications throughout water resources management. The algorithm performs its regression modeling via a meta-estimator composed of several fitted regression-based decision trees on multiple subsamples of the training data and then averages to improve the accuracy and overall robustness of prediction. We built the model using the Scikit-Learn RandomForestRegressor python package, trained using the drivers of demand identified from RFE and the OLS algorithm, and used a grid-search cross-validation function to optimize the model. We trained all models on the same data spanning 1980-2017, and omitted the three testing scenarios; wet (2008), average (2017), and dry (2015). Model evaluation leveraged percent bias (*PBias*, %), root-mean-squared-error (*RMSE*), and Kling-Gupta Efficiency Coefficient (*KGE*).

Scenario	Model	Pbias (%)	RMSE (GPCD)	KGE
Total				
	TD: Climate-Independent	-27.3	78	0.67
	CSD-WDM w/OLS	3.4	20	0.96
	CSD-WDM w/MLP	6.21	26	0.92
	CSD-WDM w/RFR	-1.45	31	0.91
Wet				
	TD: Climate-Independent	-12.1	39	0.81
	CSD-WDM w/OLS	6.04	25	0.89
	CSD-WDM w/MLP	11.6	32	0.87
	CSD-WDM w/RFR	4.48	23	0.92
Dry				
	TD: Climate-Independent	-39.7	97	0.48
	CSD-WDM w/OLS	0.2	13	0.98
	CSD-WDM w/MLP	1.98	20	0.98
	CSD-WDM w/RFR	-7.1	28	0.83
Average				
	TD: Climate-Independent	-33.4	88	0.62
	CSD-WDM w/OLS	3.31	20	0.96
	CSD-WDM w/MLP	3.86	24	0.94
	CSD-WDM w/RFR	-3.12	38	0.91

Table 4.2. The CSD-WDM with OLS regression demonstrated greater modeling performance than the more complex MLP and RFR machine learning algorithms. All machine learning algorithms demonstrate greater performance than using a historical monthly mean (TD).

While it is critical to produce accurate estimates of demand, differences in model interpretability can challenge the adoption of ML algorithms into operations. We performed a model accuracy vs. complexity evaluation that highlights a threshold of complexity for achieving representative estimates of demand. A key threshold to defining sufficient model complexity appears to depend on the integration of key, temporally dynamic service area characteristics, i.e., the integration of climate features, that produce measurable gains in model performance compared to the climate-independent econometric-based model (i.e., using historical averages to inform future demands). The high accuracy and minimal prediction error of the CSD-WDM with the OLS algorithm demonstrate that sufficient complexity can match or exceed the performance of greater complexity models (i.e., MLP, RFR).

Scenario	Model	Annual Prediction*	Annual Error*	Seasonal Prediction*	Seasonal Error*
Wet					
	TD:Climate-Independent	113500	12323	87557	10620
	CSD-WDM w/OLS	94854	-6161	74910	-2108
	CSD-WDM w/MLP	88368	-11593	68505	-7621
	CSD-WDM w/RFR	95664	-4459	75640	-511
Dry					
	TD:Climate-Independent	113500	32347	87557	24484
	CSD-WDM w/OLS	81071	-162	63155	16
	CSD-WDM w/MLP	78801	-1621	60966	-1378
	CSD-WDM w/RFR	85936	5675	68262	5918
Average					
	TD:Climate-Independent	113500	28456	87557	21808
	CSD-WDM w/OLS	81234	-2837	65019	-811
	CSD-WDM w/MLP	80990	-3243	63803	-1297
	CSD-WDM w/RFR	86746	2594	69640	4621

Table 4.3. Evaluating error in prediction at a seasonal and annual temporal resolution indicates the original OLS algorithm demonstrating the greatest average predictive performance across the three varying hydroclimate scenarios.

With the complexity vs. accuracy assessment indicating no statistically significant modeling performance benefits from the MLP or RFR algorithms, we select the CSD-WDM with the OLS regression algorithm as the demand modeling method of choice for SLCDPU. The OLS algorithm uses a linear driver-target relationship (coefficients, see Table 4.4) that supports an understanding of the factors affecting mean monthly water demands. For example, we see that for every 1°C increase in April Mean Temperature that April water demands increases by 5.63 gpcd. A key finding here is the presence of April and May mean temperature influencing demands for the remainder of the season, generally exhibiting a strong positive relationship, i.e., an increase in temperature leads to an increase in demand.

With the OLS algorithm demonstrating the greatest overall performance, we set to implement uncertainty estimates into the model. We complement the OLS algorithm with the Statsmodels v0.12.2 python package to communicate the uncertainty of the forecast to a 95% confidence level based on the internally characterized error of the model, see Figure 4.7.

Predictor	Apr	May	Jun	Jul	Aug	Sep	Oct
Population Density[1]				-0.08	-.03		
Mar LCC Streamflow[2]	0.26				15.1		
Apr LCC Streamflow[2]	0.26				0.26		
May LCC Streamflow[2]					0.26		
May BCC Streamflow[2]					11.6		
Season Snowfall[3]			0.12				
Apr Mean Temperature[4]	5.63		8.97	-3.92	3.02	4.23	
Apr Precipitation[5]	-0.31				-0.01		
May Mean Temperature[4]		14.3	14.9	9.56	-0.29	3.30	-0.5
May Precipitation[5]		-1.01					
Jun Mean Temperature[4]					1.44	-3.81	
Jun Precipitation[5]			-3.80		1.22		
Jul Mean Temperature[4]				31.2	11.5	-7.30	
Aug Mean Temperature[4]					6.32	11.96	
Aug Precipitation[5]					-1.83		
Sep Mean Temperature[4]						8.12	
Sep Precipitation[5]						-0.96	
Oct Mean Temperature[5]							5.74

[1] change in demand per $persons/km^2$

[2] change in demand per cms of streamflow (x10^{-3})

[3] change in demand per mm of snow

[4] change in demand per ^{0}C

[5] change in demand per mm of liquid precipitation

Table 4.4. The CSD-WDM uses eighteen statistically significant hydroclimate, supply, and development features to model total monthly water demands (*gpcd*).

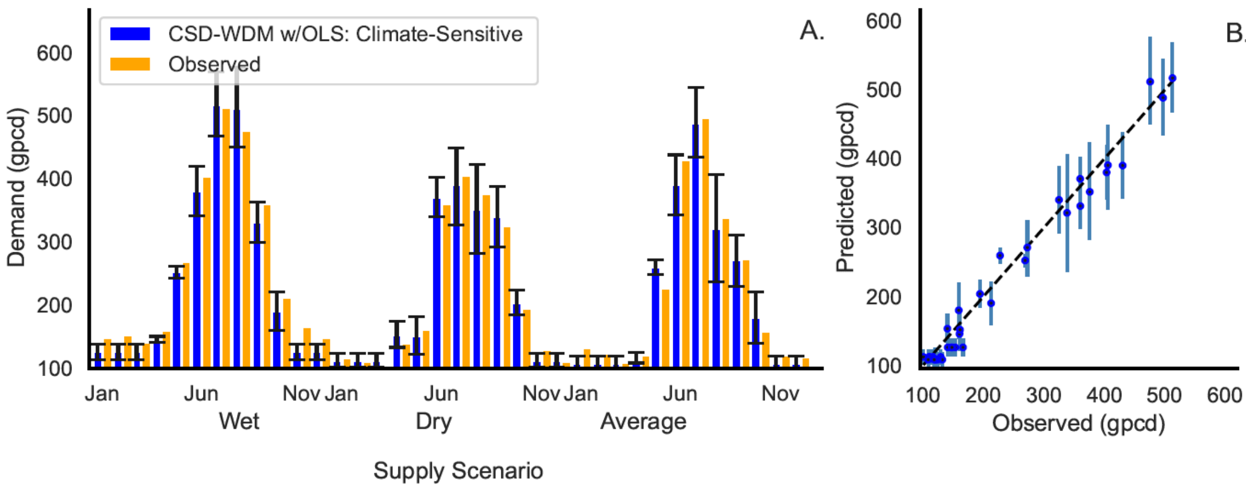

Figure 4.7: The CSD-WDM with ordinary least squares (OLS) and a 95% confidence interval demonstrates minimal error in prediction for all hydroclimate scenarios.

From the cumulative advancements and model evaluation surrounding SLCDPU demand estimation, we used the finalized model to produce estimates of demand influenced by the historical variability in observed precipitation and mean air temperature. From these simulations, we developed lookup tables in coordination with the climate and hydrology working groups, see Figures 4.8 and 4.9 for use application.

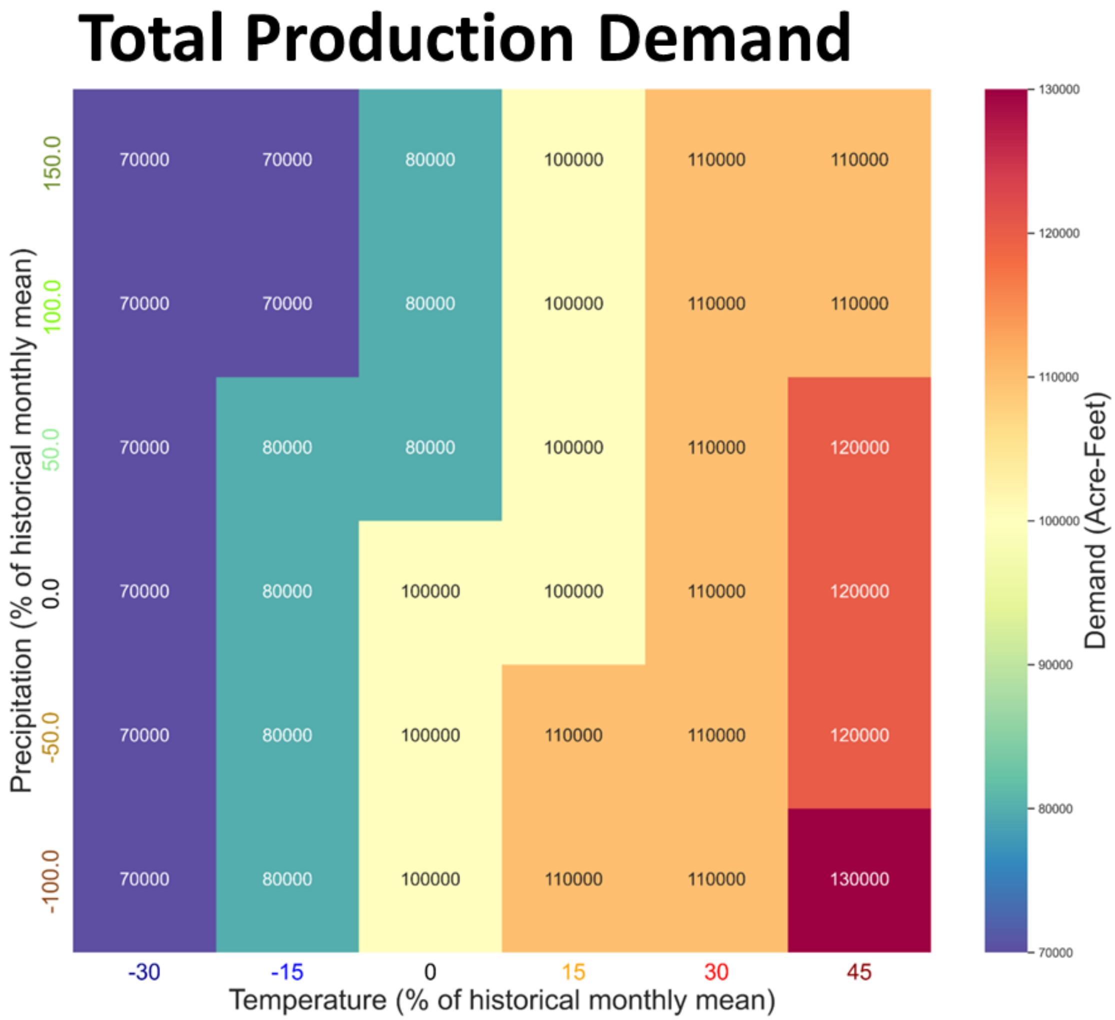

Figure 4.8: The water demand lookup table operationalizes the CSD-WDM, estimating total annual produced water demand (total volume of water needed to enter the water system, acre-feet) a function of running hundreds of simulations through the CSD-WSM with varying percentage changes in temperature and streamflow. The bounds of precipitation and temperature on the respective axes reflect the historically observed variability.

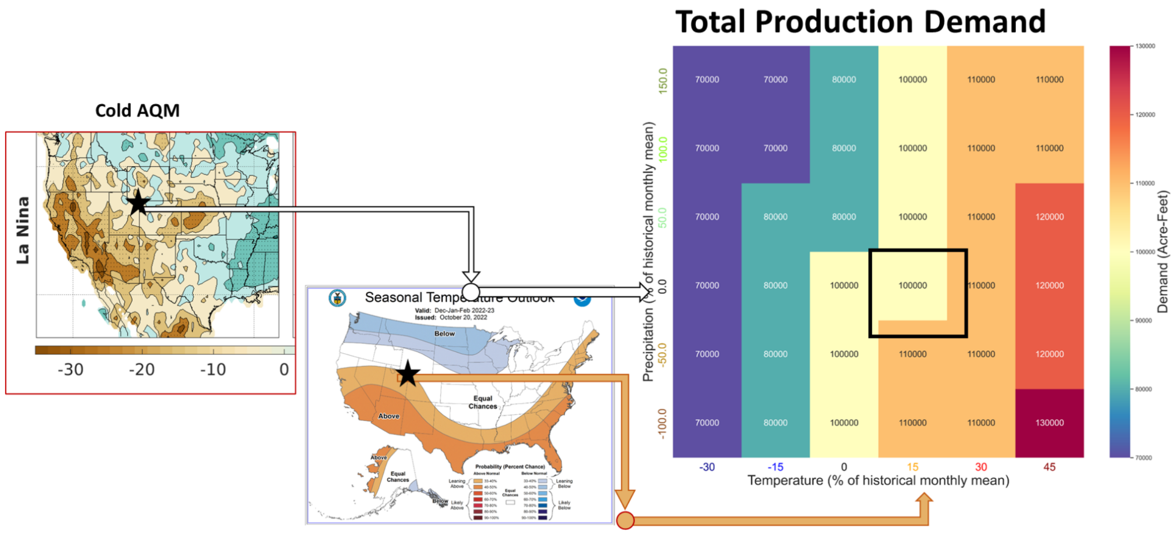

Figure 4.9: By using the AQM and ENSO phases with NOAA temperature outlooks, the table provides estimates of total annual production demand.

4.2.2 Advance modeling capabilities to guide water system management and operations

We built upon over a decade of systems model research and development enhancing the SLC-WSM to transition the modeling work into operational decision timeline components. Similar to the demand lookup table, we ran hundreds of simulations based on the availability of surface water supplies (i.e., City Creek, Parleys Creek, Big Cottonwood Creek, Little Cottonwood Creek) and projected demands (see produced water lookup tables above) to create a water system performance lookup table based on the estimated volume of Deer Creek reservoir water needed to mitigate local surface and groundwater deficits. Figure 4.10 presents the water system lookup table.

The water system performance lookup table integrates the cumulative advancements of the Climate, Hydrology, and Engineering teams. The anticipated precipitation anomaly based on the AQM and ENSO from the climate group supports streamflow estimates from the hydrology group and demand estimates from the engineering group. The total production demand estimates and streamflow supply estimates form the *x* and *y*-axis of the water system lookup table, respectively. Figure 4.11 illustrates the use of the water system performance lookup table.

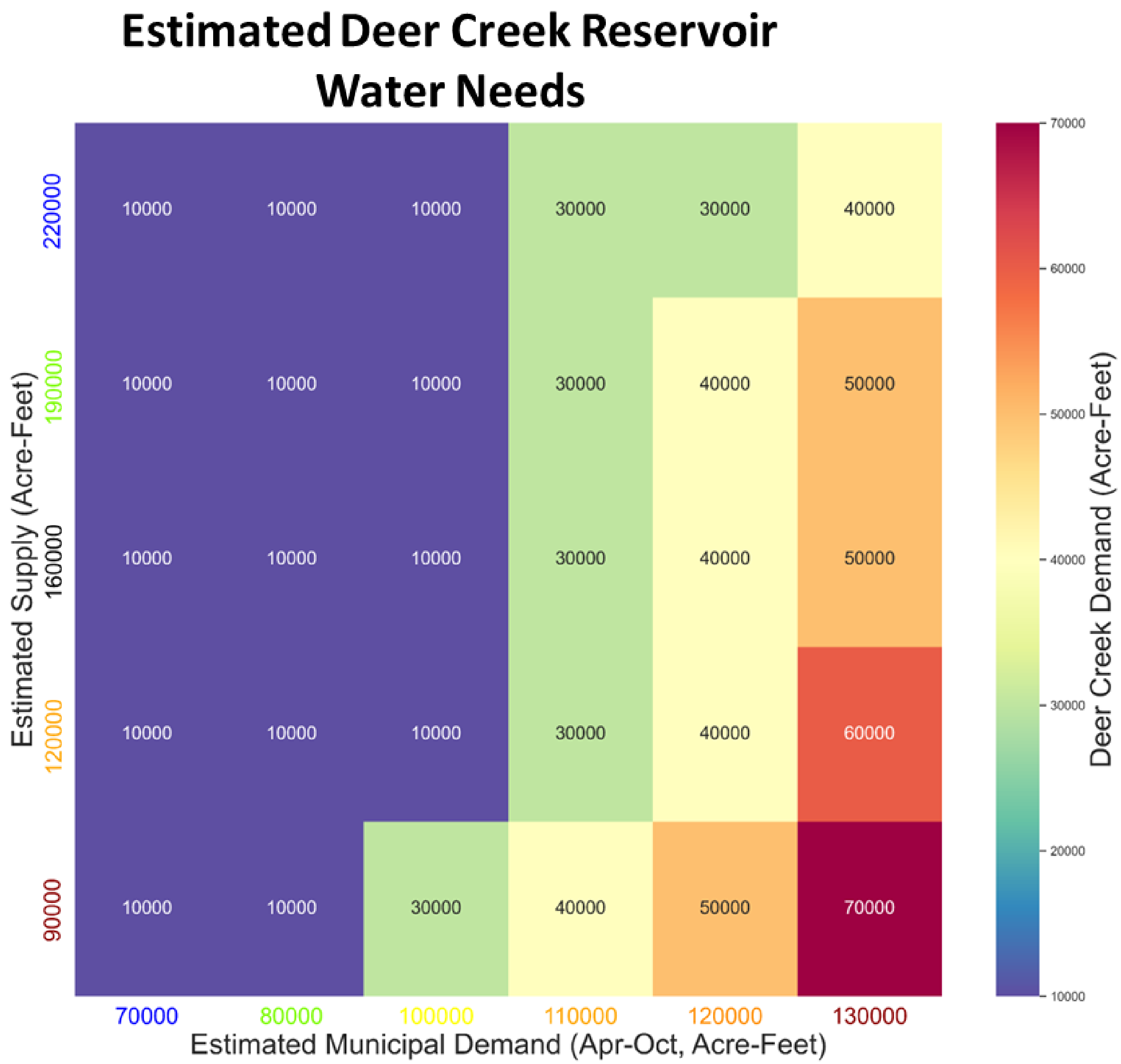

Figure 4.10: The water system lookup table leverages hundreds of water systems model (SLC-WSM) simulations of varying surface water supply and produced water demands to estimate the volume of Deer Creek reservoir water requests (acre-feet). Estimates are based on a service area population of 330,000.

The utility can use the water systems lookup tables for many applications such as: 1) event planning from SDF curves, 2) early-season planning (e.g., October), 3) mid-season planning (e.g., February - April), 4) late-season planning (e.g., June), and 5) other uses where there is a need to estimate Deer Creek water usage based on estimates of supply and demand. The primary application of the water system lookup table is for mid-season planning, as illustrated in Section 5, where there are refined estimates of supply based on observed low flows and the winter precipitation anomaly. When entering the February to April period, the utility can estimate a range of supplies and demands based on current and projected hydroclimate conditions, and by finding the respective estimates along the *x* and *y*-axis of the lookup table, can identify a range of Deer Creek water use volumes (in acre-feet) needed to prevent water system deficits.

The estimated volume of Deer Creek water provides the utility with management options. For example, if the volume of Deer Creek water is acceptable, the utility can monitor use to ensure it is aligning with the projections and meeting any carryover storage requisites. If the volume of estimated Deer Creek water exceeds an acceptable threshold, the utility can preemptively plan demand-sided conservation actions to reduce the overall volume of Deer Creek water use. Systematically using the climate, hydrology, and engineering lookup tables supports a proactive vs. reactive water system management foundation. The utility now has significantly reduced uncertainty in the volume of annual supply, demand, and system water needs to develop management actions that mitigate potential supply-demand deficits and maximize carryover storage capacity.

5. Synthesis

The research-to-operations partnership between the Salt Lake City Department of Public Utilities, the University of Utah, and the University of Alabama has led to key scientific advancements in western precipitation anomaly, improving the fundamental understanding of Wasatch Mountain hydrology, and novel methods for transitioning research advancements to actionable water resources management tools. While each of these advancements reduces the uncertainty of managing SLCDPU's water resources, the realized benefit of the research is the ability to create an operational decision timeline. Figure 5.1 illustrates the timing of reliable estimates of water system performance influencing components (i.e., supply and demand).

The decision timeline begins with an estimation of the anticipated western US precipitation anomaly for the upcoming water year beginning in October. At this time, there is sufficient confidence in the winter ENSO pattern and, while in development, the AQM to form preliminary estimates of above-average, average, or below-average winter precipitation quantities. The steps in Section 2.3 describe the process for forming statistically informed early season estimates of the quantity of water year precipitation.

Early winter presents the next opportunity in the operational decision timeline where statistically significant models relate antecedent hydrological conditions to estimate catchment annual water yield. A key indicator driving the models is antecedent groundwater storage, assessed using January baseflow. While there is uncertainty in melt rate and melt duration, the projections of winter precipitation and observations of catchment baseflow reduce the overall uncertainty of annual catchment water yield by roughly half (for example, from 30k -200k acre-feet to 120k-160k acre-feet). In this step, the utility can use the climate lookup tables to estimate annual precipitation or refer to catchment SNOTEL observations to estimate a winter precipitation trajectory. Using the precipitation estimates and baseflow observations supports estimates of annual catchment yield while reducing the overall uncertainty.

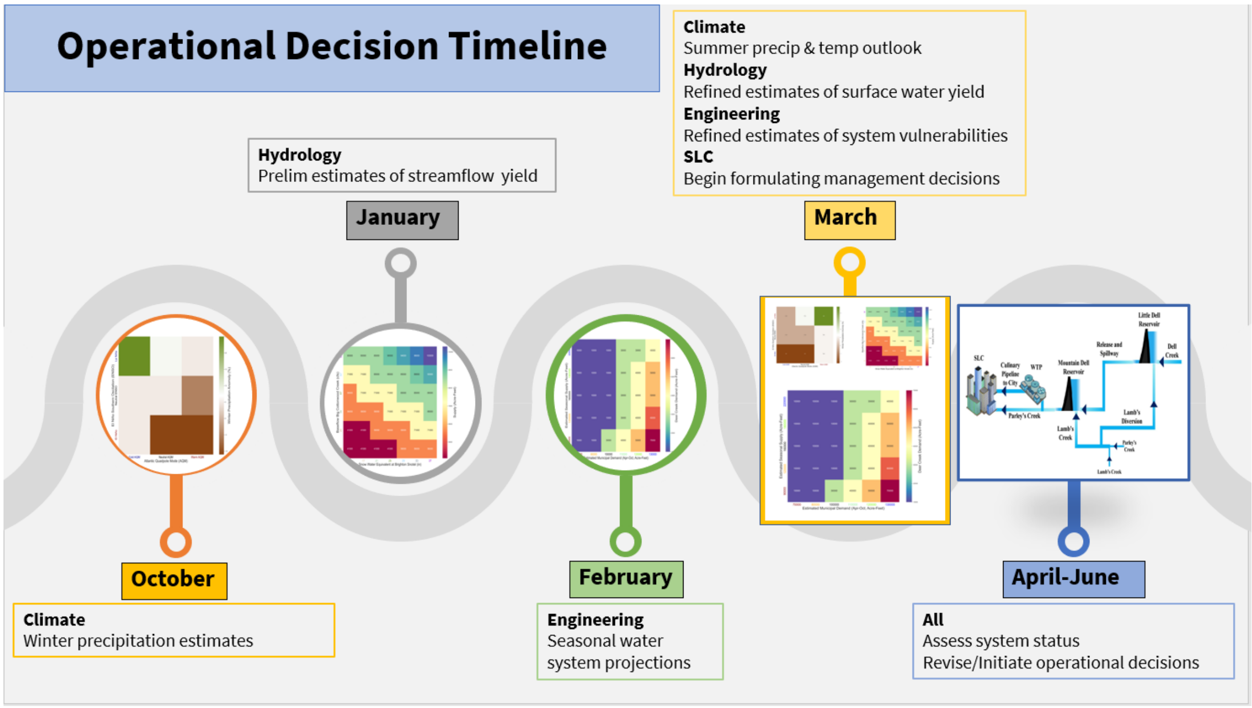

Figure 5.1. A Decision Timeline Framework to guide water resources decision-making.

Developing proactive approaches to water system operations and decision-making leverages the advancements in the SLC-WSM in replicating surface water supply, municipal water demand, and water system infrastructure limitations and interactions. In the operational decision timeline, we need estimates of annual surface water supply and water demand to understand water system interactions for identifying potential vulnerabilities and developing mitigation measures. Through extensive conversation with the utility, the volume of Deer Creek reservoir water serves as a vulnerability indicator of water system performance due to the increased treatment, pumping, and it being a shared resource among other municipalities. With the framework for generating surface supply estimates above, there is a need for estimating water demand to estimate water system performance.

Following a framework similar to the winter precipitation and surface water supply tables, we provide total produced water demand estimates using the relationships between service area temperature and precipitation. Beginning in February, NOAA provides seasonal temperature and precipitation outlooks that can form inputs into the water demand lookup table (i.e., April and May temperature and precipitation probabilities). NOAA provides estimates based on the probability of an event rather than a given quantity, which requires the utility to make an inference connecting the probability of an event to a range in precipitation quantities and temperatures. For example, if the NOAA seasonal forecast suggests a high probability of above-average temperatures, the utility could explore all above-average temperatures. The same mindset can be applied to precipitation. Note, the range of percent-from-average values in the demand lookup table covers the range of values within the historical record (i.e., 1980-2020).

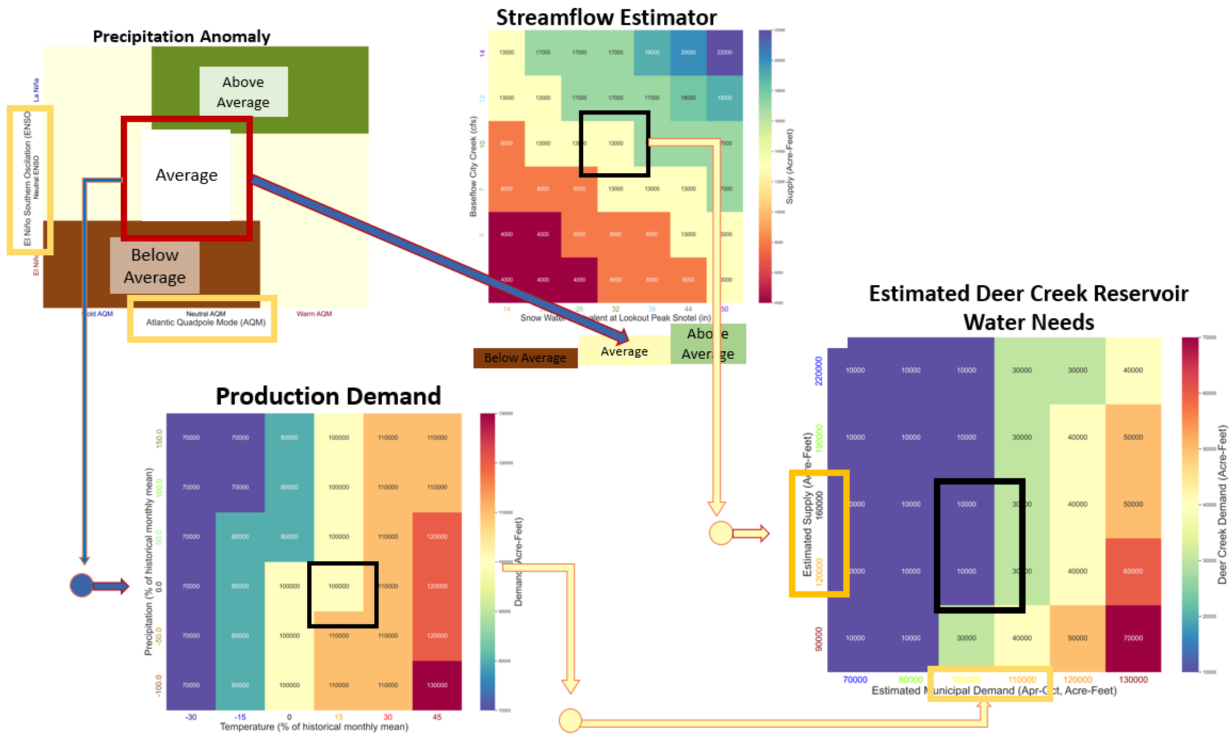

Figure 5.2: The water systems lookup table leverages surface water supply (i.e., streamflow) and production demand estimates using the AQM and ENSO precipitation anomaly. The workflow estimates Deer Creek reservoir water needs to prevent supply deficits.

With estimates of annual surface water supply and total produced water needs by February, the utility can produce their first estimates of annual Deer Creek Reservoir Water needs using the respective water system lookup table (Figure 4.10). The lookup table supports proactive water system management, leveraging the research, knowledge, and modeling to produce a data-informed tool for estimating the volume of Deer Creek Reservoir water needs as an indicator of water system performance. While there is little actionable operational component to increasing or decreasing supply availability, the lookup table provides the ability to make generalized demand hedging estimates (i.e., is conservation needed to avoid a predetermined threshold of Deer Creek water use? Should the utility propose drought contingency plans to increase carry-over capacity?) Figure 5.2 displays the above-described workflow for initiating climate-supply-demand-water system performance estimation.

The final phase of the operational decision timeline is evaluation. While the lookup tables containerized the climate, hydrology, and engineering research based on historical observation and climate simulation, there is uncertainty in every model and corresponding estimate. It is also difficult to take the breadth of information, simulations, and results into a comprehensive lookup table that takes into account nonstationarity and the climate variability within the region. Thus, from the time of initial estimates to June, we recommend the utility revisiting the table and adjust the inputs as the uncertainty in the estimates are reduced. For example, by May, we will have surpassed peak SWE and thus will have reduced the uncertainty in winter precipitation quantity. Similarly, we will know how April and May temperatures relate to the historical average which has a very strong influence on annual produced water demands. Lastly, NOAA releases its summer temperature and precipitation guidance in May, supporting refined estimates of water demand. With reduced uncertainty in supply and demand, and better estimates of reservoir levels from the CBRFC, the utility can have refined estimates of water system performance to inform decision-making.

6. References

Eyring, V., S. Bony, G. A. Meehl, C. A. Senior, B. Stevens, R. J. Stouffer, and K. E. Taylor (2016), Overview of the Coupled Model Intercomparison Project Phase 6 (CMIP6) experimental design and organization, Geosci. Model Dev., 9(5), 1937-1958, doi: 10.5194/gmd-9-1937-2016.

Horan, M. F. and T. Reichler (2017): Modeling Seasonal Stratospheric Sudden Warming Climatology Based on Polar Vortex Statistics, *Journal of Climate*, 30(24), 10101-10116.

McCabe, G. J., M. A. Palecki, and J. L. Betancourt (2004), Pacific and Atlantic Ocean influences on multidecadal drought frequency in the United States, Proceedings of the National Academy of Sciences, 101(12), 4136-4141, doi: 10.1073/pnas.0306738101.

Pedregosa et al. (2011) Scikit-learn: Machine Learning in Python, Journal of Machine Learning Research, 12, pp. 2825-2830.

Tebaldi, C., et al. (2021), Climate model projections from the Scenario Model Intercomparison Project (ScenarioMIP) of CMIP6, *Earth System Dynamics*, 12(1), 253-293, doi: 10.5194/esd-12-253-2021.

Stone, L. (2022) Pacific and Atlantic drivers of winter precipitation over the Continental United States, Master's Thesis, University of Utah.

Wise, E. K. (2010), Spatiotemporal variability of the precipitation dipole transition zone in the western United States, Geophys Res Lett, 37(7), doi: 10.1029/2009GL042193.

Wolf, M. and coauthors (2023) Multi-year Climatic Controls on Groundwater Storage in Seasonally Snow-Covered Headwater Catchments, Water Resources Research, in revision.

Zhang, R., Sutton, R., Danabasoglu, G., Kwon, Y.-O., Marsh, R., Yeager, S. G., et al. (2019). A review of the role of the Atlantic Meridional Overturning Circulation in Atlantic Multidecadal Variability and associated climate impacts. *Reviews of Geophysics*, 57, 316– 375. https://doi.org/10.1029/2019RG000644.

7. Appendices

Appendix A.1 Climate Vulnerability Project Glossary (alphabetical)

Baseflow – Streamflow derived from groundwater storage

CAM - Community Atmosphere Model

Catchment storage - consists of both groundwater (below gravitational water table) and soil moisture/ vadose zone water storage

CESM - Community Earth System Model

Clausen, B., & Pearson, C. P. (1995). Regional frequency analysis of annual maximum streamflow drought. *Journal of Hydrology*, *173*(1-4), 111-130.

CMIP – Coupled Model Intercomparison Project https://gmd.copernicus.org/articles/9/1937/2016/

Dracup, J. A., Lee, K. S., & Paulson Jr, E. G. (1980). On the statistical characteristics of drought events. *Water resources research*, *16*(2), 289-296.

EMMA – End Member Mixing Analysis is a method for determining dominant flow paths and/or runoff sources contributing to streamflow using dissolved solute concentrations; http://snobear.colorado.edu/Markw/WatershedBio/EMMA/burns_01.pdf

FDOM – Fluorescent Dissolved Organic Matter is a continuous (for our permanent) measurement of organic matter content of a solution (stream water). FDOM is a tracer of water movement through shallow soils

MCA - Maximum Covariance Analysis is a method of statistical analysis that objectively finds patterns of covariation between two large data sets (e.g., Atlantic sea surface temperatures and western-US precipitation).

Mishra, V., Cherkauer, K. A., & Shukla, S. (2010). Assessment of drought due to historic climate variability and projected future climate change in the midwestern United States. *Journal of Hydrometeorology*, *11*(1), 46-68.

PDSI – Palmer Drought Severity Index; https://climatedataguide.ucar.edu/climate-data/palmer-drought-severity-index-pdsi

PHDI – Palmer Hydrologic Drought Index; https://www.ncdc.noaa.gov/temp-and-precip/drought/historical-palmers/overview

Quadpole -- a pattern of climate anomalies made up of four regions arranged north to south. Similar terms exist for single regions (monopole), two regions (dipole), and three regions (tripole). In our application, the Atlantic Quadpole is a pattern of sea surface temperature anomalies which influences study-region precipitation.

R2O - Research to Operations

RCP - Representative Concentration Pathway https://en.wikipedia.org/wiki/Representative_Concentration_Pathway

Runoff Efficiency/ Water Yield – a dimensionless fraction relating the amount of water existing a catchment as surface water (Q) divided by the amount of precipitation that fell over a period of time (usually water year

SDF Approach – An integration measure of drought and potential water shortage combining Severity, Duration, and Frequency

SpC – Specific Conductance is an integrated (and for our permanent sites) continuous measure of total dissolved solutes

SPEI – Standardized precipitation Evapotranspiration Index; https://climatedataguide.ucar.edu/climate-data/standardized-precipitation-evapotranspiration-index-spei

SPI – Standardized Precipitation Index; https://climatedataguide.ucar.edu/climate-data/standardized-precipitation-index-spi

SSP - shared socioeconomic pathways (greenhouse gas emission scenarios for CMIP6, analogous to RCPs used in CMIP5) https://climateanalytics.org/media/gmd-13-3571-2020.pdf

SST - sea surface temperature

Storm flow – The fraction of discharge associated with a runoff event (precipitation or melt) that is not derived from baseflow. Stormflow is calculated as total discharge - baseflow

Appendix A.2 Project publications and conference presentations

Publications:

Wolf, M.A, Jamison, L.R, Solomon, D.K, Strong, C, and Brooks, P.D. (In Revision). Multi-year Controls on Groundwater Storage in Seasonally Snow-Covered Headwater Catchments. *Water Resources Research.*

Brooks, P. D., Gelderloos, A., Wolf, M. A., Jamison, L. R., Strong, C., Solomon, D. K., et al. (2021). Groundwater-mediated memory of past climate controls water yield in snowmelt-dominated catchments. *Water Resources Research*, 57, e2021WR030605. https://doi.org/10.1029/2021WR030605

Johnson, Ryan C.; Wolf, Margaret; Jamison, Logan; Burian, Steven; Oroza, Carlos A.; Brooks, Paul D.; Strong, Courtenay; Stewart, Jesse; and Kirkham, Tracie (2021) Drought in the West: Embedded Water Demand Stationarity Compromises System Vulnerability Analysis, *Open Water Journal*: Vol. 7 : Iss. 1 , Article 6. https://scholarsarchive.byu.edu/openwater/vol7/iss1/6

Conference presentations:

Brooks P, Gelderloos A, Wolf M, Jamison L, Solomon K, Strong C, Burian S, Tai X, 2019. When S does not equal 0:A multi-year climate signal, mediated through groundwater, controls annual water yield in seasonally snow-cover ed mountain headwaters, American Geophysical Union Fall Meeting, San Francisco, California, 9-13 December 2019.

Brooks P, Ehleringer J, Bowen B, Bowen G, Bowling D, Briefer L, Follstad-Shah J, Hinners S, Lin J, Pataki D, Strong C, Mackenzie Skiles S, Solomon DP, Steenburgh J, 2019. Red Butte Creek and the Wasatch Environmental Observatory: A mountain to urban research facility in the semi-arid Western US, American Geophysical Union Fall Meeting, San Francisco, California, 9-13 December 2019.

Brooks PD, Gelderloos A, Wolf MA, Jamison LR, Strong C, Solomon DK, Bowen GJ, Briefer L, 2021. Predicting snowmelt-derived water resources in a changing climate: Warming and multi-year droughts reduce runoff efficiency by depleting groundwater storage and slowing melt, American Geophysical Union Fall Meeting, New Orleans, Louisiana, 13-17 December 2021.

Brooks PD, Strong C, Wolf M, Johnson RC, Aziz D, Steward J, Burian SJ, Jamison LR, Stone L, Kirkham T, Briefer L, 2022. Climate, Hydrologic, and Systems Modeling to Assess Water Supply Changes to Climate Change, American Geophysical Union Fall Meeting, Chicago, Illinois, 12-16 December 2022.

Johnson R, Burian SJ, Halgren J, Aziz D, Strong C, Stone L, Brooks P, Wolf M, Jamison L, Briefer L, Kirkham T, Stewart J, Prue Tamara, 2023. Research to Operations Stakeholder Engagement to Mitigate Water System Climate Vulnerabilities, *American Meteorological Society Annual Meeting,* Denver, CO, 9 January 2023.

Wolf MA, Jamison LR, Solomon DK, Strong C, Brooks PD, 2021. A 12-Catchment Comparison of How Multi-year Climate Controls Catchment Recharge, Storage, and Streamflow Using Over a Century of Data in Northern Utah, American Geophysical Union Fall Meeting, New Orleans, Louisiana, 13-17 December 2021.

Wolf M, Jamison L, Strong C, Solomon DK, Brooks PD, 2021. A 12 Catchment Comparison of How Multi-year Climate Controls Catchment Storage, Recharge and Streamflow Using Over a Century of Data in Northern Utah (Poster). American Geophysical Union (AGU).

Wolf M, 2021. Quantifying the Effect of Ongoing Drought in Northern Utah Streamflow. Salt Lake County Watershed Symposium. (Presentation).

Wolf M, Jamison LR, Strong C, Brooks P, 2022. Perturbations of groundwater storage in headwater catchments of the Upper Colorado River Basin: Improving our understanding of why runoff in mountain environments is so variable, American Geophysical Union Fall Meeting, Chicago, Illinois, 12-16 December 2022.

Wolf M, Jamison L, Gelderloos A, Strong C, Solomon DK, Brooks PD, 2019.. Snowmelt runoff efficiency mediated through multi-year climatic controls on groundwater recharge in the Wasatch Mountains, Utah, USA (Poster). American Geophysical Union (AGU).

Appendix A.3 Streamflow Lookup Tables for Water Supply Catchments

Estimated Water Supply (Acre Ft) for Big Cottonwood using Baseflow and Peak SWE

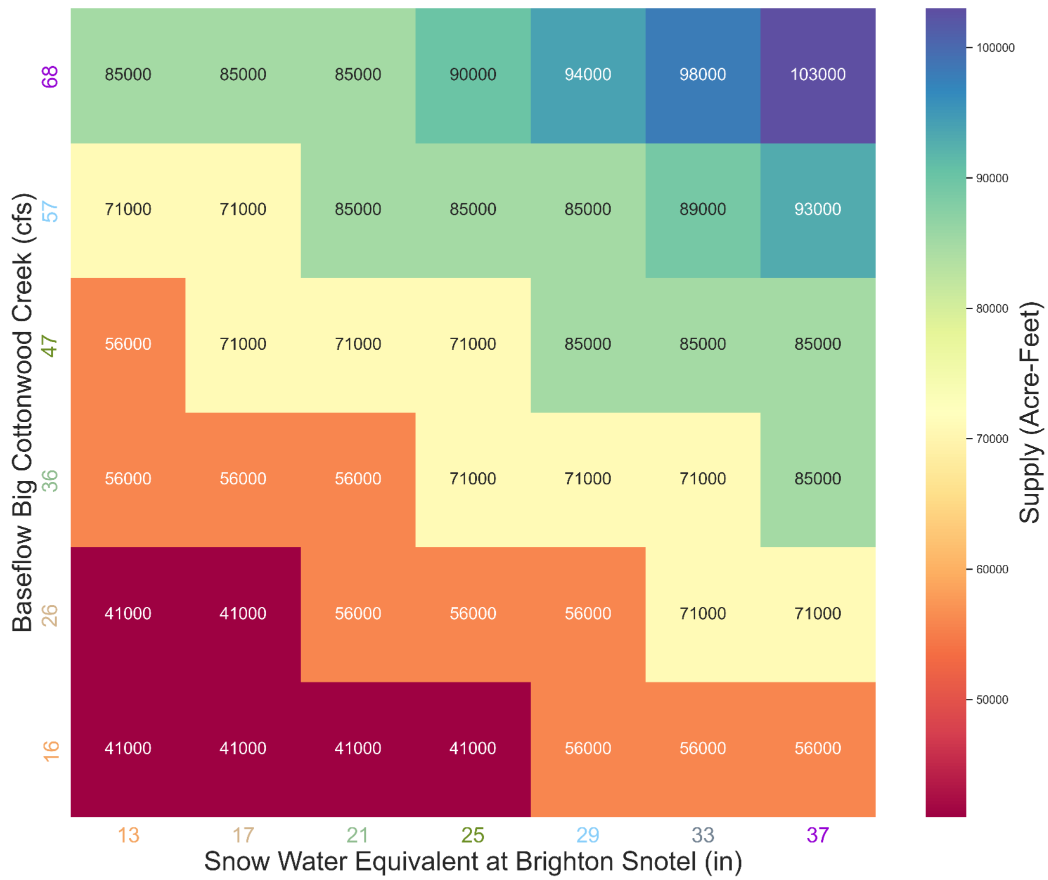

Estimated Water Supply (Acre Ft) for Little Cottonwood Creek using Baseflow and Peak SWE

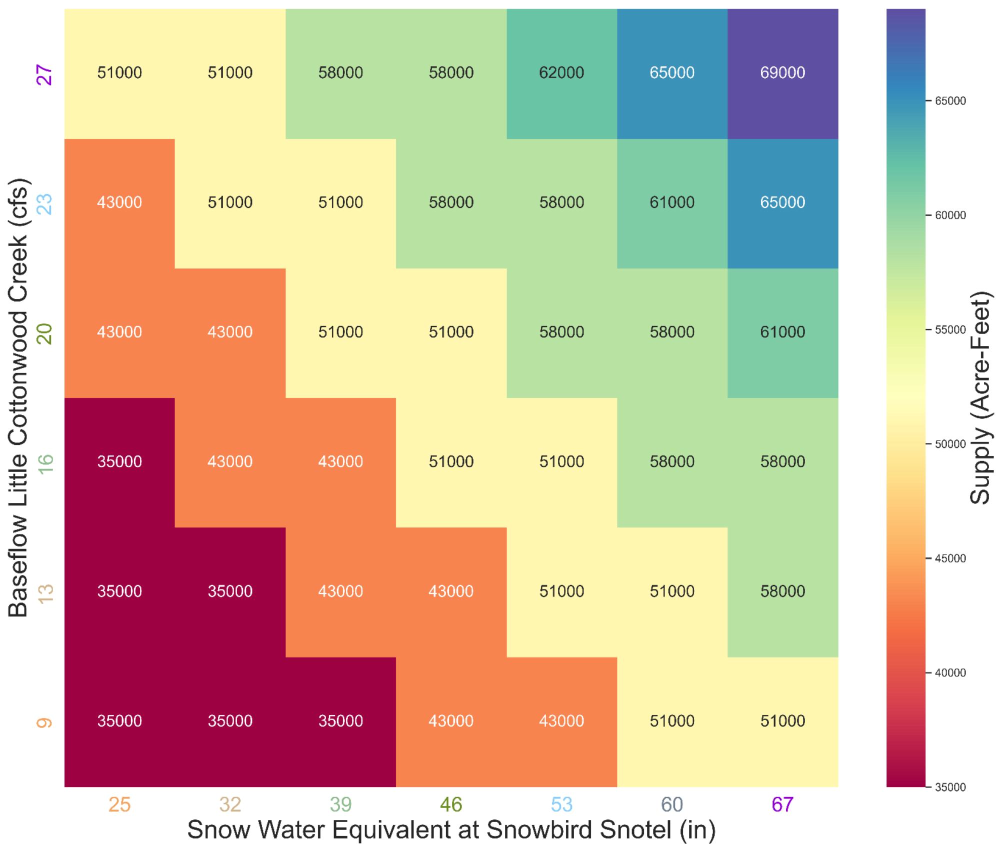

Estimated Water Supply (Acre Ft) for Parleys Creek using Baseflow and Peak SWE

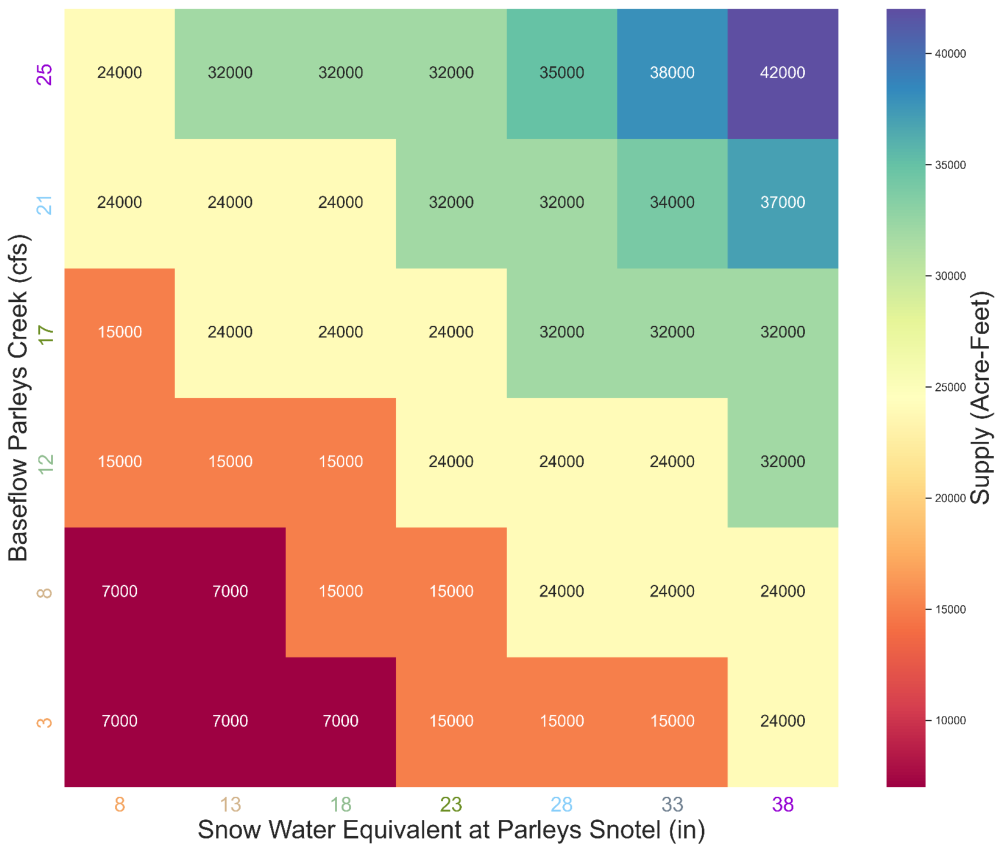

Estimated Water Supply (Acre Ft) for City Creek using Baseflow and Peak SWE

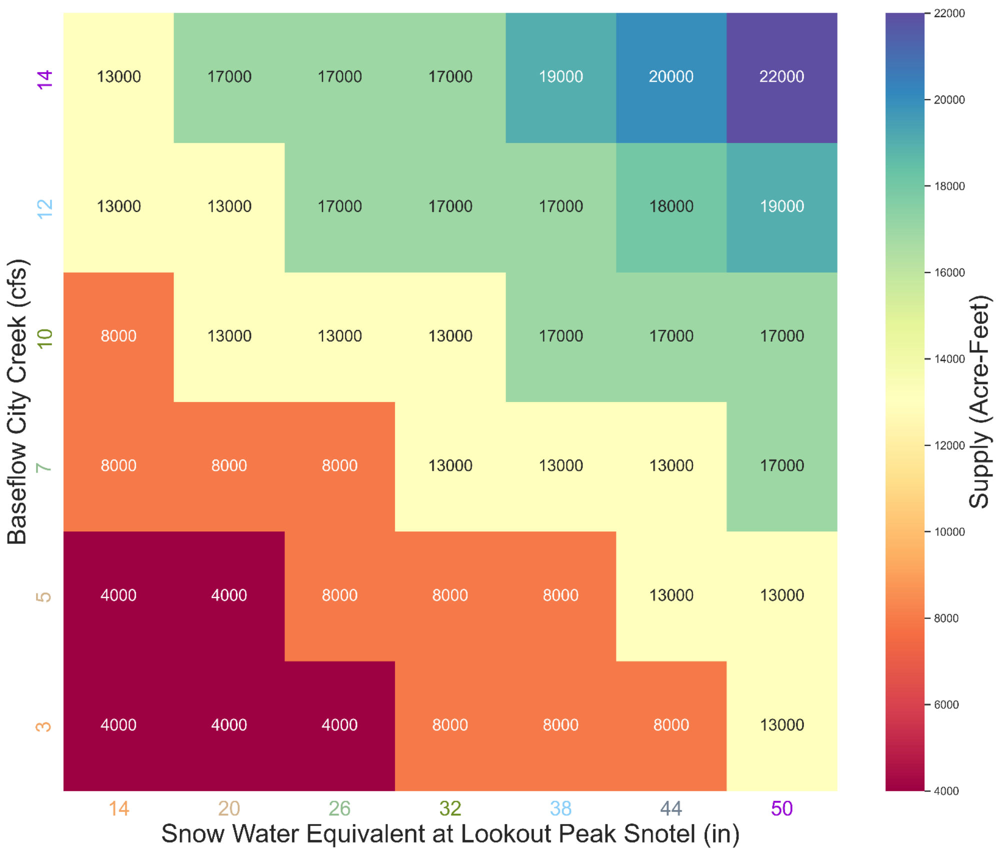

Appendix A.4 Red Butte Creek Long Term Discharge and Hydrochemistry

Introduction and Study Location

Red Butte Creek's (RBC) headwaters originate in the Wasatch Mountains east of Salt Lake City in a highly protected Research Natural Area (RNA) with restricted access and very little impact from human development. The creek flows westward through the RNA, the University of Utah campus, and Salt Lake City before it joins the Jordan River and ultimately reaches the southern end of the Great Salt Lake. This provides a unique opportunity to research how water supply and water quality vary along this headwater-to-urban transition.

The Red Butte monitoring network consists of four climate sites and seven aquatic sites (Figure A.4.1, Table A.4.1). Sites above the Red Butte Reservoir lie within the RNA and are representative of the natural environment. Sites below the reservoir are affected by human management, with the impact from development generally increasing downstream. All aquatic sites are instrumented with sensors to measure discharge and several water chemistry parameters that are indicative of water quality and can be used to "fingerprint" streamwater. By quantifying the interaction time between the water, the subsurface, and shallow soils, we can make inferences about the source and relative age of streamwater. Climate sites are instrumented with sensors to measure a variety of climate parameters, but the two basic parameters presented in this report are air temperature and precipitation. All data is collected at 15-minute intervals and may be aggregated to daily, monthly, or annual values (water year, Oct. 1 – Sept 30). To evaluate water supply metrics, we used aquatic data from headwater sites in Upper RBC (LKF and ARBR). To quantify water quality, we used aquatic data from urban sites below the reservoir (RBG, CG, FD, 1300E, and 900W).

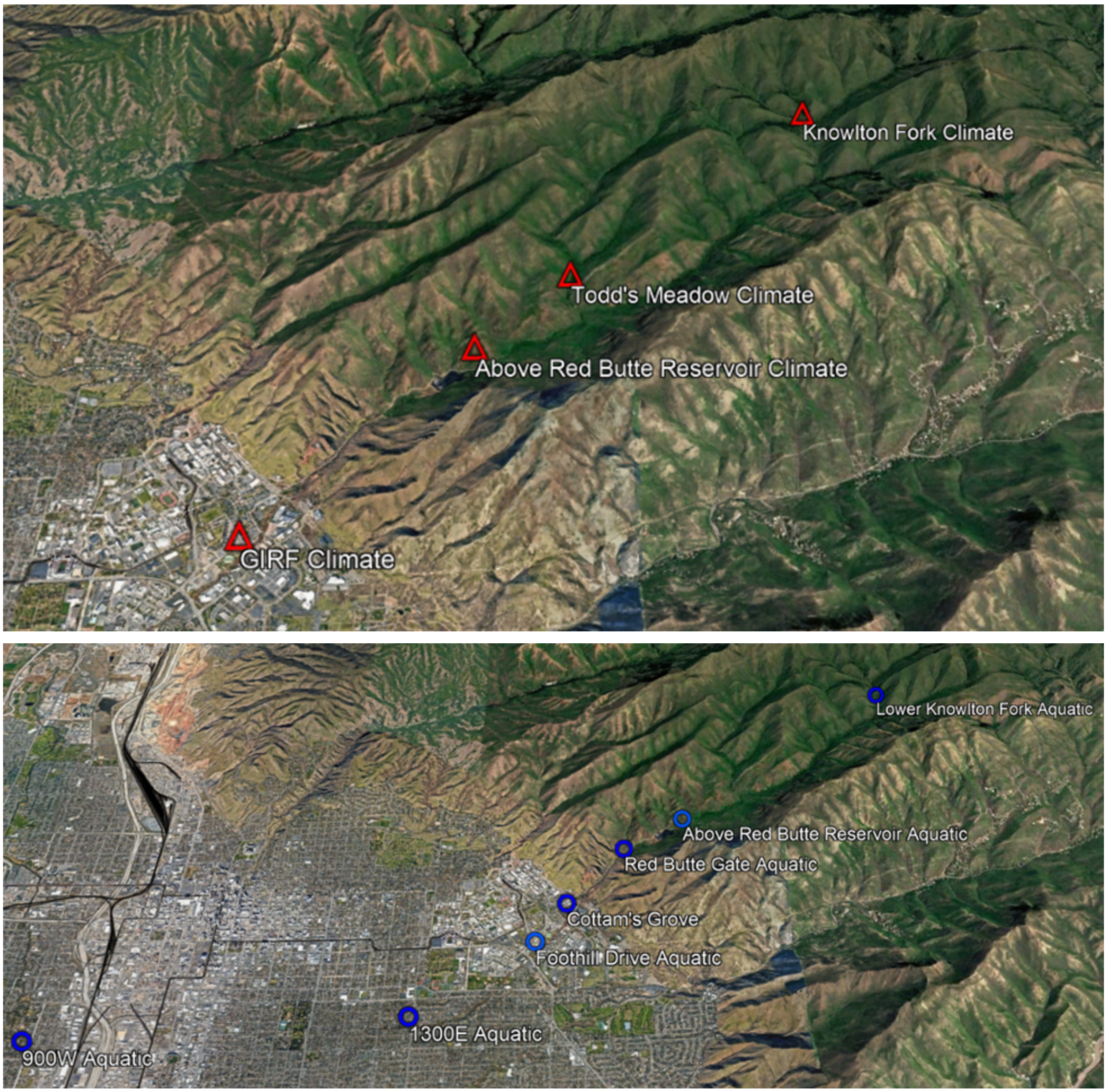

Figure A.4.1: Map of climate (top) and aquatic (bottom) monitoring sites along Red Butte Creek.

Site Name	Abbreviation	Latitude/Longitude	Elevation (m)
Knowlton Fork Climate	RB_KF_C	40.789054°,-111.796416°	2178
Todd's Meadow Climate	RB_TM_C	40.789054°,-111.796416°	1763
Above Red Butte Reservoir Climate	RB_ARBR_C	40.780567°, -111.807222°	1666
Green Infrastructure Research Facility (GIRF) Climate	RB_GIRF_C	40.760800°,-111.830474°	1487
Lower Knowlton Fork Basic Aquatic	RB_LKF_BA	40.805550°, -111.765467°	1942
Above Red Butte Reservoir Advanced Aquatic & USGS gauge	RB_ARBR_AA	40.779602°,-111.806669°	1649
Red Butte Gate Basic Aquatic	RB_RBG_BA	40.774050°,-111.817798°	1582
Cottams Grove Basic Aquatic	RB_CG_BA	40.763958°, -111.828286°	1502
Foothill Drive Advanced Aquatic	RB_FD_AA	40.757225°, -111.833722°	1449
1300E Aquatic	RB_1300E_A	40.745000°, -111.854433°	1353
900W Basic Aquatic	RB_900W_BA	40.741583°, -111.917650°	1289

Table A.4.1: Red Butte Creek climate and aquatic monitoring site names, abbreviations, locations, and elevations.

Water Supply in Upper RBC

The climate and hydrology of the headwaters of RBC are similar to mountain catchments throughout the intermountain west, which are characterized by relatively hot, dry summers, and cold, snowy winters, resulting in the accumulation of seasonal snowpacks that melt in spring as solar radiation increases. Streamflow is typically relatively stable and low throughout the year (except for isolated storm events) until snowmelt begins and streamflow increases. Streamflow remains elevated during snowmelt before receding to baseflow levels once the snowpack has melted out. The cycle of snowpack accumulation, snowmelt, and the resulting melt-induced streamflow is relied upon as the most important component of water resources in western North America.

Rapid population growth and climate change will stress Utah's already limited water supply. It is uncertain exactly how higher air temperatures will affect water resources in seasonally snow-covered headwater catchments, but the expectation is reduced water supply and a shift towards earlier timing of snowmelt-induced streamflow. RBC is relatively warm and dry compared to other water supply catchments in the Salt Lake City area and may be used to draw inferences about how water resources in colder and wetter catchments may respond to future warming. Understanding the sources and relative age of streamwater in upper RBC will allow water managers to assess the vulnerability of water supplies to climate change, and on what time scales hydrologic changes might occur.

Variability in RBC water supply is predominantly controlled by annual precipitation amount (Brooks et al., 2021). Mean annual precipitation at RBC sites from water years 2015-2021 ranges from 47 cm (GIRF_C) to 87 cm (KF_C), with mean annual precipitation increasing by 5.4 cm for every 100 m gained in elevation (Figure 2). Similarly, mean annual air temperature ranges from 11.7˚C (GIRF_C) to 6.5˚C (KF_C) and decreases by 0.74˚C for every 100 m gained in elevation. Daily climate data and monthly average data are included in the summary tables at the end of this appendix.

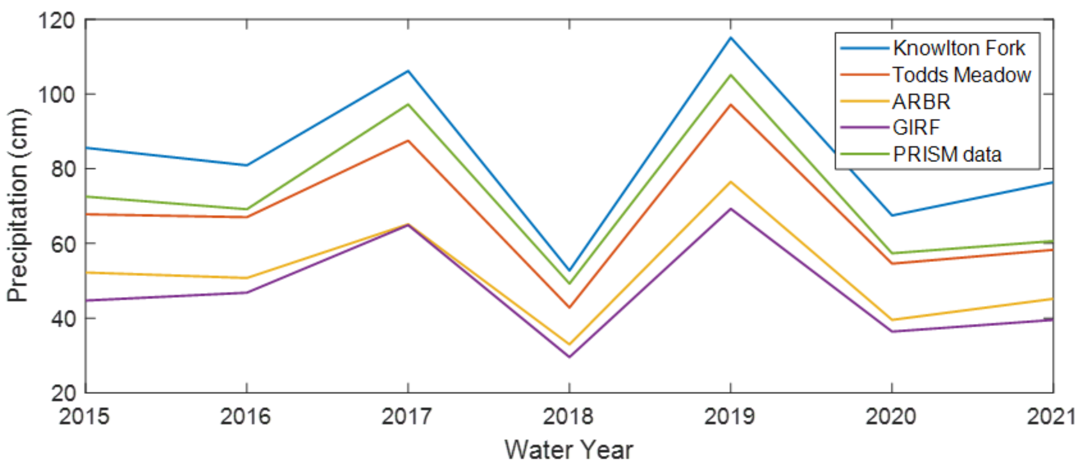

Figure A.4.2: Water years 2015-2021 annual precipitation at Red Butte Climate Sites. Area-weighted mean PRISM precipitation data for the watershed (above USGS gauge/ARBR site) is also included for reference. Interannual variability in precipitation and temperature is consistent across sites.

Unsurprisingly, discharge in Upper RBC increases as you move downstream. Similar to precipitation and temperature, variability in discharge is consistent across sites (Figure 3). However, human management at the reservoir impacts discharge at the RBG site, which is immediately downstream of the dam.

Due to several gaps in discharge data across all sites (including the USGS gauge at ARBR), linear interpolation was used to fill data gaps so that total annual streamflow volume could be calculated. These data gaps were typically during periods of low flows, such that unknown errors due to linear interpolation of data likely have minimal impacts on the calculation of annual discharge volume. Unfortunately, at RBG site, several longer gaps in discharge data (including during periods of higher flows) made calculating annual discharge volume unfeasible for several years. As a result, comparisons of runoff efficiency only include LKF and ARBR. Because discharge is altered by human management at RBG, runoff efficiency calculations at that site are less indicative of the natural environment anyways, compared to LKF and ARBR sites.

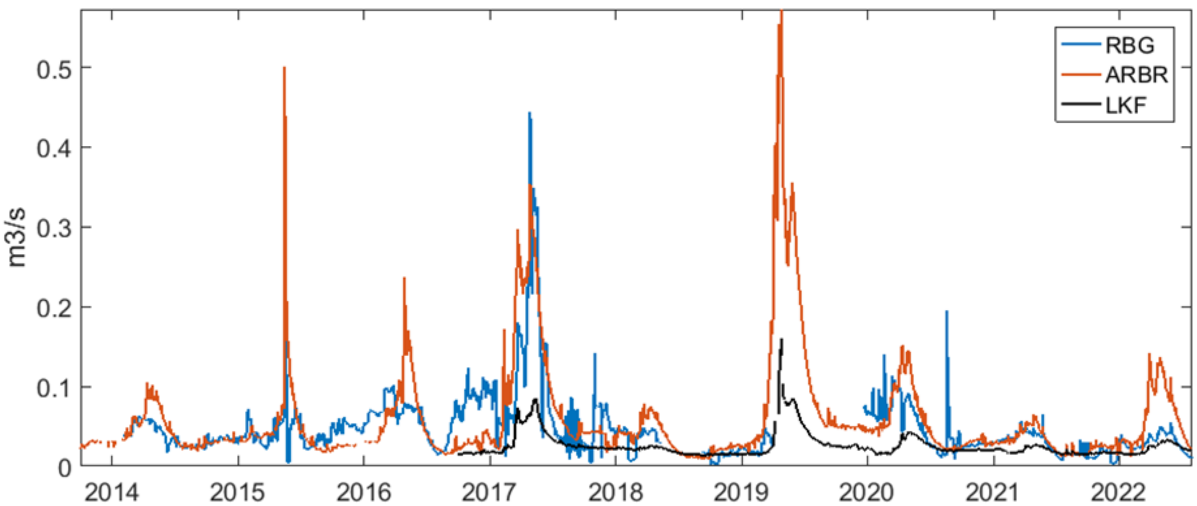

Figure A.4.3: Daily discharge at upper RBC sites. Streamflow is generally low for much of the year but increases sharply with the onset of snowmelt. RBG is included here for reference, but note that discharge at RBG is affected by dam management, and often has a different pattern of streamflow compared to LKF and ARBR.

Runoff efficiency (the ratio of annual streamflow to precipitation) is a useful metric to determine how effectively precipitation is partitioned to streamflow, such that catchments with higher runoff efficiencies more effectively generate streamflow from a given precipitation amount compared to catchments with lower runoff efficiencies. To calculate runoff efficiency at upper RBC sites, total annual streamflow in m^3 was first normalized for watershed area to yield units comparable to precipitation (mm). Additionally, PRISM precipitation data were used instead of precipitation data from individual climate sites. PRISM data is likely more indicative of precipitation amounts in the entire upstream area of each site, as opposed to precipitation from point locations at climate sites. The area-weighted mean of all PRISM pixel values above individual sites (LKF and ARBR) was calculated for each month and summed to water year values.

Runoff efficiency for water years 2017-2021 ranges from 0.27 to 0.36 at LKF and for water years 2015-2021 ranges from 0.11 to 0.19 at ARBR (Table 2). Runoff efficiency is consistently higher at LKF compared to ARBR, indicating that streamflow generation is more efficient at the higher elevations of the watershed. However, interannual variability in runoff efficiency is less consistent across sites than discharge. Interestingly, runoff efficiency in LKF was actually highest in the relatively dry water years of 2018 and 2020 (following the wet years of 2017 and 2019). In contrast, runoff efficiency is higher at ARBR during wetter years. This variability in runoff efficiency from upstream to downstream suggests spatial variability in how precipitation is partitioned and that the source of streamwater may be variable from upstream to downstream. Note the very low runoff efficiency at ARBR in water year 2021, indicating that 92% of the precipitation that fell was partitioned to either evapotranspiration or to recharging groundwater.

Runoff Efficiency		
	LKF	ARBR
2015		0.11
2016		0.12
2017	0.28	0.17
2018	0.34	0.12
2019	0.28	0.19
2020	0.36	0.17
2021	0.27	0.08

Table A.4.2: Water years 2015-2021 runoff efficiencies at LKF and ARBR sites.

Stream chemistry provides additional insight into the relative sources and age of streamwater in Upper RBC. Specific conductance (SpCond) is a measure of a water's ability to conduct an electrical current and is indicative of the total ion concentration in water. Water that has had greater interaction with the subsurface (i.e. groundwater) will have a higher ion concentration and thus a higher specific conductance value than fresh precipitation or snowmelt. For example, fresh snowmelt typically has a specific conductance value of less than 30 uS/cm, while groundwater values may range from roughly 300 to over 3,000 uS/cm (USGS Techniques and Methods 9-A6.3, 2019).

Timeseries of daily SpCond values at ARBR and LKF (Figure A.4.4) indicate that streamwater at both sites is primarily sourced from subsurface water that has a much higher ion concentration than fresh snowmelt. SpCond values at LKF are relatively stable throughout the year but decrease slightly during snowmelt in the two highest snowfall years (2017 and 2019). At ARBR, streamwater during the winter months has even higher values of SpCond compared to LKF, indicating that older groundwater sustains low flows down canyon (mean monthly SpCond values in appendix). During the snowmelt season, SpCond at ARBR decreases rapidly as dilution occurs, but SpCond values (~400-500 uS/cm) are still far greater than those of fresh snowmelt. Taken in combination with the runoff efficiencies presented previously, these results suggest that streamwater in the highest portion of RBC is primarily composed of subsurface water (that may be carried over from the previous year), while further downstream, streamwater is composed of older groundwater during periods of low flows and a mixture of old and new waters during snowmelt.

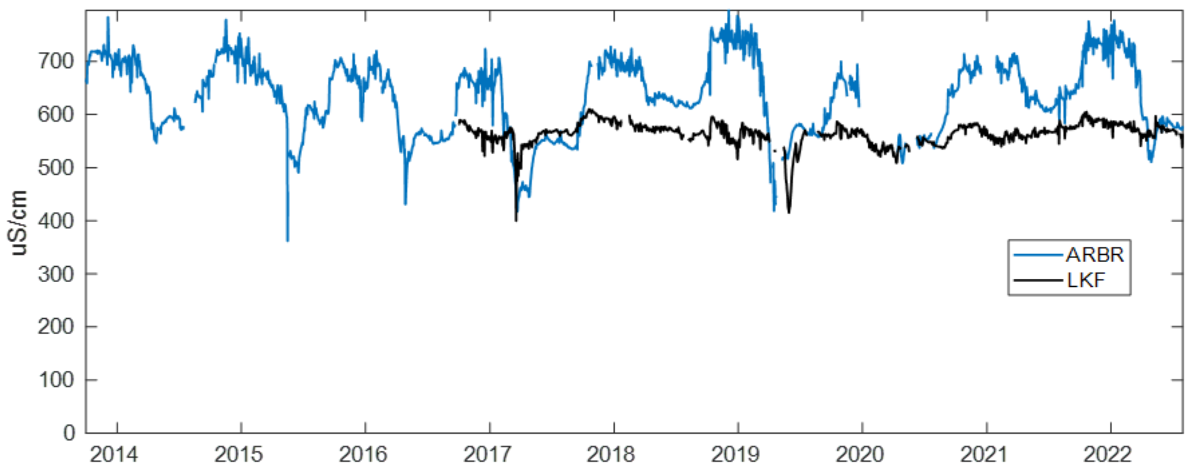

Figure A.4.4: Daily specific conductance values (uS/cm) at LKF and ARBR sites, indicating that streamflow is primarily sourced from subsurface water with some mixing of new water during snowmelt.

Using a very simple end member mixing model, we approximate the fraction of "old" (subsurface water, higher SpCond) and "new" (fresh snowmelt/precipitation, lower SpCond) water in RBC. The mixing model is of the form:

$$Qs\,Cs = QnCn + QoCo$$

where Qs is the discharge in the stream, Q_n is the discharge that comes from the new water, Q_o is the discharge that comes from old water, C_s is the ion concentration (approximated by SpCond) measured in the stream, C_n is the ion concentration of the new water endmember, and C_o is the ion concentration of the old water endmember. Assuming that C_o equals the maximum SpCond recorded at each site (representative of ion concentration of groundwater) and that C_n equals 5 uS/cm (approximate SpCond value of fresh snow), we rearrange the equation above to solve for Q_n (where $Q_o = Q_s - Q_n$):

$$Qn = (Qs(Cs - Co))/Cn - Co$$

Solving this equation indicates that the vast majority of streamwater in upper RBC is sourced from "old" water (i.e. groundwater) and only during snowmelt and intense precipitation events is there a significant amount of "new" fresh snowmelt or rainfall entering the stream (Figure 5). Even during snowmelt, less than 30% of the water at ARBR and less than 20% of the water at LKF is fresh snowmelt. It is important to note that these results are highly dependent on the values of the end members chosen. Further constraining the end member values (via groundwater and snow sampling) will yield more accurate results.

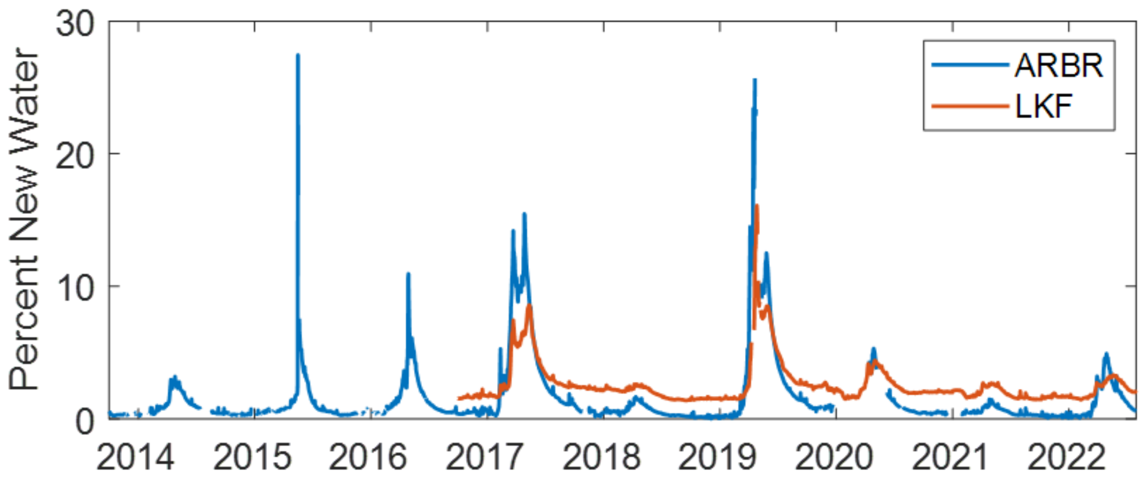

Figure A.4.5: Timeseries showing the estimated percent of new (fresh snowmelt or rain) water in RBC at ARBR and LKF sites. The vast majority of streamwater in upper RBC is derived from subsurface water, even during the snowmelt season.

Fluorescent dissolved organic matter (fDOM) is another useful water chemistry parameter to source streamwater. fDOM is indicative of how much interaction water has had with soil, as soils have a relatively high organic matter content compared to fresh snowmelt or precipitation. Comparing fDOM values with discharge at ARBR site, we see elevated fDOM values during periods of higher streamflow, including during snowmelt (Figure A.4.6). These results indicate that streamwater has passed through the soil before reaching the stream channel. Notably, during snowmelt, there is a slight lag between fDOM and discharge, such that fDOM values increase rapidly prior to peak streamflow. This result suggests there is a "flushing" of stored soil water prior to peak snowmelt. fDOM values are also typically high during the fall season (monthly mean fDOM values in appendix), likely due to the abundance of leaf litter in the stream and on soil surfaces.

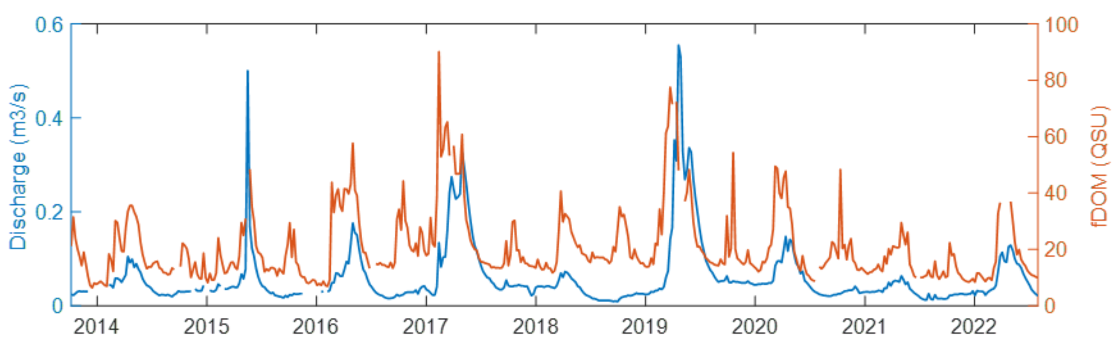

Figure A.4.6: Time series of weekly discharge (blue) and fDOM (orange) values at ARBR site. Increases in fDOM during snowmelt and periods of high discharge indicate streamwater has passed through soils before reaching the stream channel.

The results presented above highlight the importance of stored subsurface water to water supply in RBC, suggesting that streamflow during snowmelt is a mixture of stored groundwater, flushed soil water, and a relatively small fraction of fresh snowmelt. The physical mechanisms controlling this “displacement” of older water during snowmelt are not well-constrained. Previous work (Brooks et al., 2021; Wolf et al. and others) indicate that variability in subsurface storage is controlled by antecedent climate (mainly the previous years’ snowfall) and that storage variability may have an increasing influence on water supply as the climate warms. Water supply in RBC (and other SLC supply catchments) is especially vulnerable to consecutive years of below-average snowfall, even if none of those consecutive years are extremely low. This can be seen in water year 2021, where 2021 precipitation was only slightly below-average, but due to below-average precipitation in 2020, streamflow in 2021 was far below that of 2020. The low snowfall during 2020 was likely not enough to recharge groundwater, thus making the activation of stored water during 2021 snowmelt less effective. However, variability in other hydroclimate metrics not considered in this study (evapotranspiration, melt dynamics, etc.) likely influence the surprisingly low streamflow generation in 2021 as well.

The Red Butte Creek climate and aquatic stations record 15 minute interval data measurements. Below is a snapshot of the water quality measurements taken at the lower Red Butte Canyon sites from 2014-2022 including, daily discharge(Q), specific conductance(SpCond), pH, dissolved oxygen(DO), dissolved organic matter(fDOM) and Nitrate-N.

Water Quality in Lower RBC

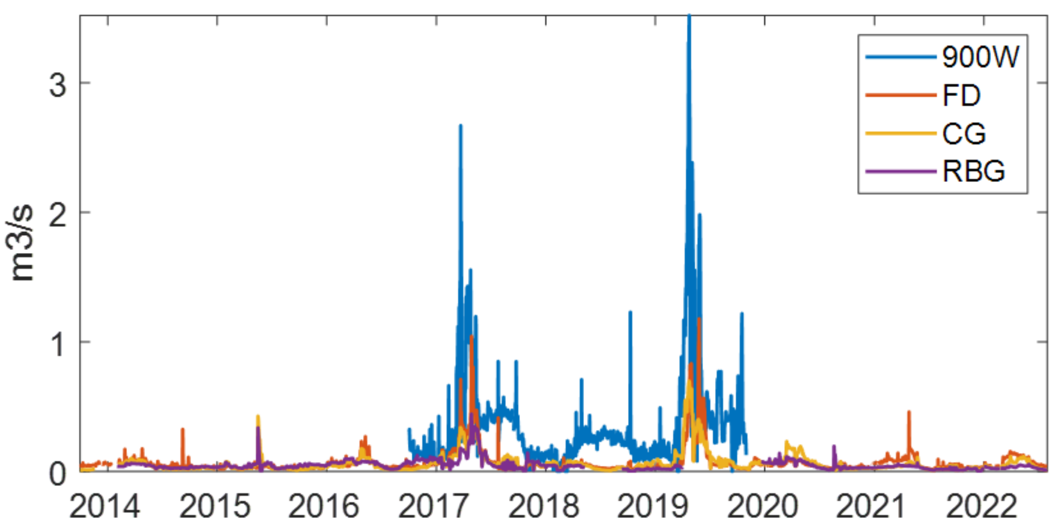

Figure A.4.7: Daily discharge at Lower RBC sites. Discharge generally increases downstream and the hydrograph becomes much more “flashy” due to precipitation falling on impervious surfaces and entering the stream channel rapidly through storm drains.

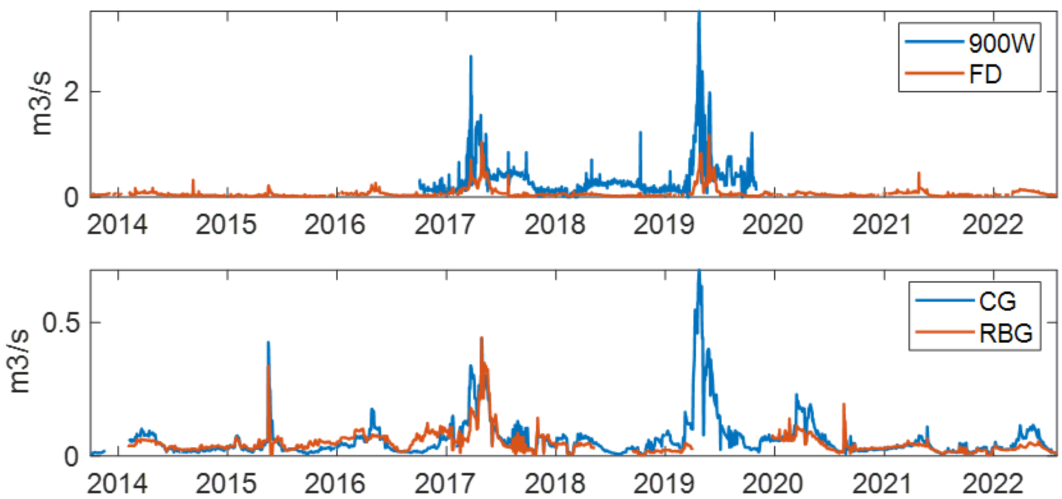

Figure A.4.8: Daily discharge at Lower RBC sites (separated into two panels). Discharge generally increases downstream and the hydrograph becomes much more "flashy" due to precipitation falling on impervious surfaces and entering the stream channel rapidly through storm drains.

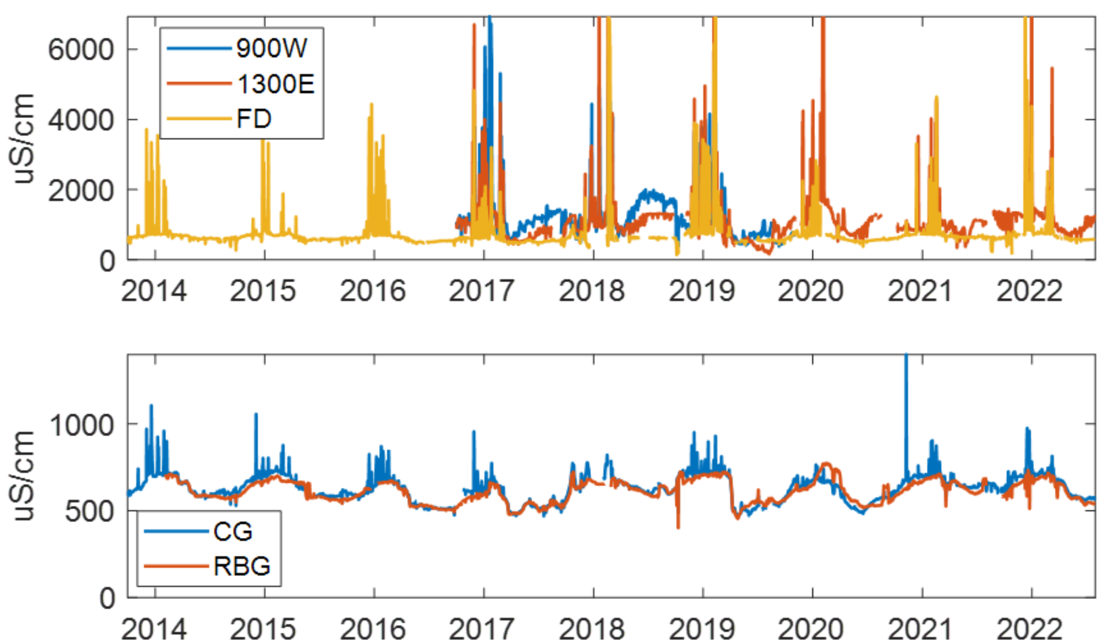

Figure A.4.9: Daily specific conductance at Lower RBC sites (separated into two panels for clarity). SpCond values at downstream sites are typically similar during summer low flows, but increase dramatically during winter storms as road salts and other contaminants are flushed into the stream.

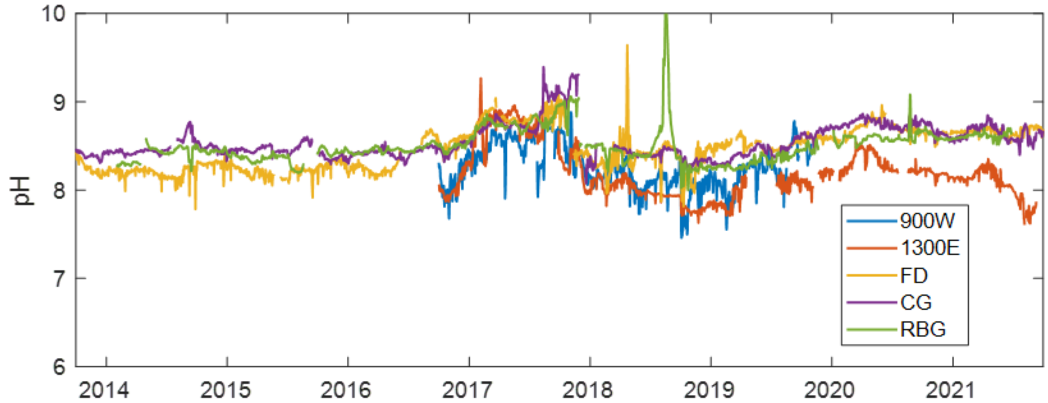

Figure A.4.10: Time series of daily pH values in Red Butte Creek.

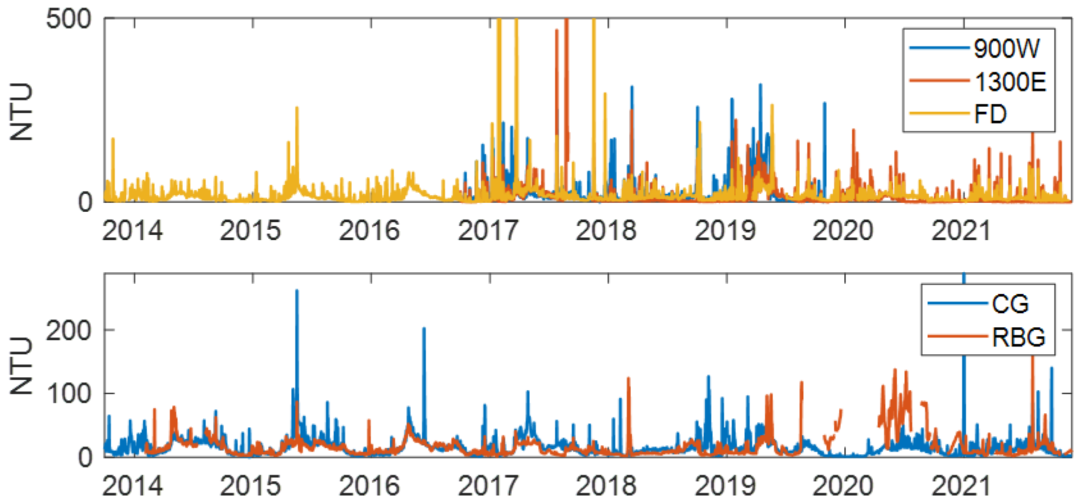

Figure A.4.11: Daily turbidity values (NTU) at Lower RBC sites (separated into two panels for clarity). A few very high values at FD and 1300E extend past the y-axis limit on the top figure.

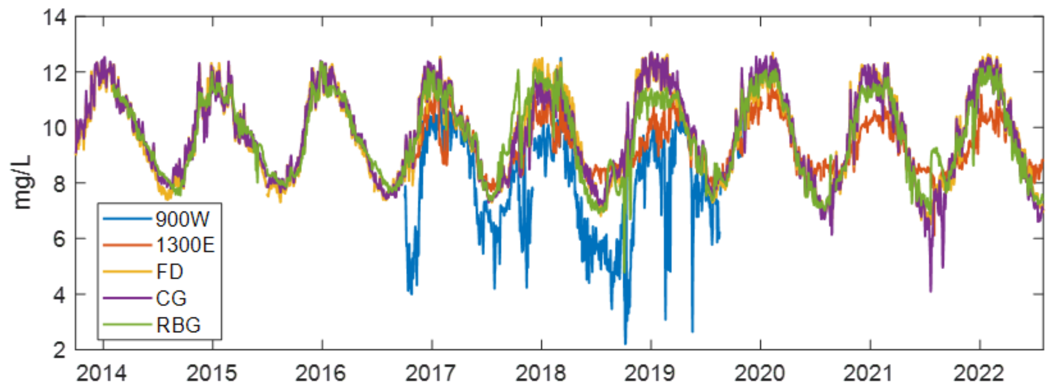

Figure A.4.12: Daily dissolved oxygen (mg/L) values at Lower RBC sites. Dissolved oxygen at 900W drops low enough in summer months to not support cold water aquatic species.

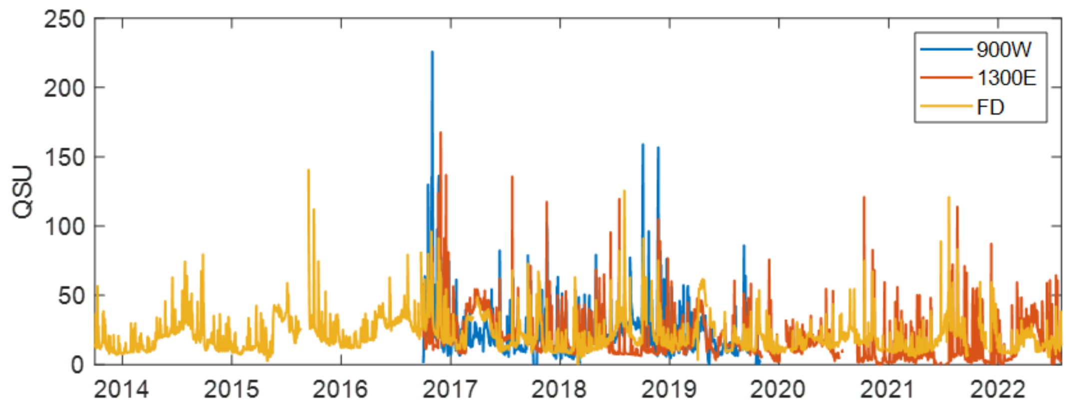

Figure A.4.13: Daily fDOM (Dissolved Organic Matter) (QSU) values at Lower RBC sites.

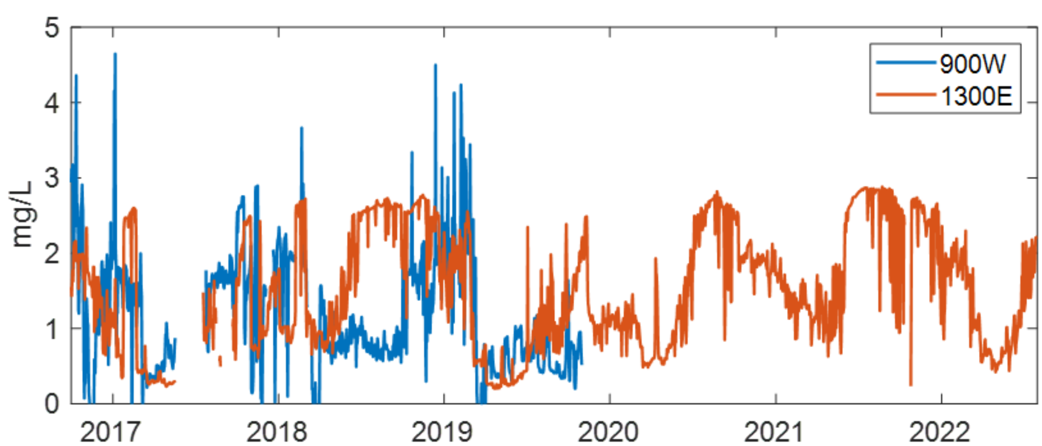

Figure A.4.14: Daily Nitrate-N (mg/L) values at Lower RBC sites.

Red Butte Creek Summary Tables

	KF_C	TM_C	ARBR_C	GIRF_C
January	10.2	7.2	5.2	4.8
February	9.4	6.9	4.8	4.4
March	9.8	8.7	6.3	6.4
April	8.9	8.7	6.5	6.0
May	8.8	7.4	6.2	5.3
June	2.7	2.4	1.8	1.5
July	2.1	1.6	1.4	1.2
August	3.7	3.4	3.1	2.8
September	5.5	5.2	4.5	4.2
October	5.8	5.4	4.3	4.0
November	6.5	4.7	3.3	2.8
December	11.1	8.5	5.8	5.5

Table A.4.3: Mean monthly accumulated precipitation (cm) across all years at RBC climate sites.

	KF_C	TM_C	ARBR_C	GIRF_C
January	-3.3	-2.8	-1.3	-0.3
February	-2.6	-1.5	0.3	1.9
March	1.2	2.9	4.9	6.7
April	4.2	6.1	8.0	9.8
May	9.0	10.1	12.4	14.3
June	15.1	15.8	19.4	21.8
July	18.2	19.5	23.9	26.0
August	17.2	18.3	22.5	24.5
September	13.1	13.7	17.2	19.0
October	5.9	6.8	9.2	11.0
November	1.0	1.8	4.0	5.4
December	-3.6	-3.4	-1.7	-0.5

Table A.4.4: Mean monthly air temperature (C) across all years at RBC climate sites.

	LKF	ARBR	RBG	CG	FD	1300E	900W
January	565	704	675	708	1056	1471	2073
February	560	688	694	712	1107	1946	1812
March	555	648	662	669	701	1027	1113
April	553	576	611	609	616	781	767
May	553	572	576	571	571	706	962
June	556	576	564	559	563	817	1209
July	562	581	559	570	573	943	1291
August	560	584	563	584	571	978	1328
September	567	618	562	576	575	1057	1189
October	583	690	602	637	637	1076	995
November	580	700	631	664	751	1216	1038
December	571	698	653	700	1088	1410	1489

Table A.4.5: Mean monthly SpCond values (uS/cm) across all years at Red Butte Creek sites. SpCond is typically lowest during the snowmelt season and highest from late summer through winter. Even during the snowmelt season, streamwater SpCond is much higher than that of freshly melted snow, indicating mixing of fresh snowmelt and older stored water. Very high SpCond values at downstream sites in winter may be due to salt from roads washing into the stream via storm drains.

	LKF	ARBR	RBG	CG	FD	1300E	900W
January	8.35	8.41	8.47	8.47	8.42	8.15	8.19
February	8.37	8.43	8.47	8.53	8.43	8.17	8.17
March	8.41	8.35	8.47	8.56	8.45	8.30	7.91
April	8.43	8.39	8.46	8.57	8.51	8.37	8.35
May	8.45	8.44	8.50	8.55	8.48	8.36	8.28
June	8.38	8.49	8.49	8.51	8.47	8.25	8.26
July	8.34	8.47	8.49	8.51	8.46	8.18	8.24
August	8.32	8.48	8.63	8.61	8.51	8.03	8.26
September	8.35	8.49	8.56	8.65	8.54	8.08	8.44
October	8.26	8.46	8.52	8.56	8.44	8.06	8.13
November	8.31	8.43	8.52	8.56	8.40	8.09	8.16
December	8.36	8.39	8.46	8.47	8.43	8.10	8.20

Table A.4.6: Mean monthly pH values across all years at Red Butte Creek sites.

	ARBR	FD	1300E	900W
January	12.7	12.6	14.9	19.3
February	20.9	15.1	13.8	19.5
March	33.3	16.7	21.9	20.6
April	36.3	22.2	26.7	24.5
May	28.8	22.0	21.9	21.3
June	17.7	21.8	14.8	17.0
July	14.3	25.7	14.0	19.1
August	14.2	27.5	16.7	21.0
September	17.2	23.2	14.0	25.0
October	24.9	27.0	15.6	30.1
November	16.0	21.3	19.7	40.8
December	13.0	16.5	15.3	22.5

Table A.4.7: Mean monthly fDOM values (QSU) across all years at Red Butte Creek sites. ARBR site (the only site in this table unimpacted by human management) shows higher fDOM values during snowmelt season, suggesting the activation of stored soil water during melt.

	LKF	ARBR	RBG	CG	FD	1300E	900W
January	9.0	6.3	7.7	12.1	37.9	17.3	46.5
February	9.9	4.9	7.2	8.5	17.2	14.3	24.9
March	9.2	10.7	11.5	11.6	18.8	19.8	48.0
April	13.6	30.5	23.5	22.6	24.5	24.8	43.6
May	9.2	16.9	27.9	28.6	32.9	25.1	43.1
June	6.8	6.8	19.4	19.9	19.4	14.7	11.9
July	5.8	6.7	19.0	17.1	14.9	11.0	15.0
August	4.6	3.1	20.2	19.4	14.9	33.2	13.1
September	2.9	2.9	23.2	19.2	14.2	5.6	16.8
October	2.0	2.7	10.8	12.0	10.3	8.7	19.4
November	5.0	1.8	9.6	7.2	9.3	4.8	16.1
December	5.7	2.0	13.5	9.6	11.7	7.5	18.6

Table A.4.8: Mean monthly turbidity values (NTU) across all years at Red Butte Creek sites.

	LKF	ARBR	RBG	CG	FD	1300E	900W
January	10.7	12.0	11.5	11.8	11.8	10.4	9.6
February	10.6	11.8	11.3	11.6	11.6	10.2	8.9
March	10.3	11.1	10.9	10.9	10.9	10.4	9.6
April	10.0	10.4	9.9	10.1	10.0	9.8	9.3
May	9.5	9.6	9.0	9.2	9.1	9.0	7.5
June	9.2	9.0	8.3	8.2	8.1	8.4	6.7
July	9.0	8.3	7.7	7.5	7.5	8.3	6.4
August	9.0	8.4	8.2	7.8	7.8	8.4	6.0
September	9.2	9.0	8.3	8.3	8.3	8.6	7.1
October	9.6	9.9	9.1	9.4	9.3	8.9	6.3
November	10.1	11.2	10.5	10.6	10.6	9.3	7.2
December	10.6	11.9	11.3	11.6	11.7	10.2	9.3

Table A.4.9: Mean monthly dissolved oxygen values (mg/L) across all years at Red Butte Creek sites. DO levels at most sites are high enough to sustain cold-water aquatic species year-round, while at 900 W DO often drops below 6 mg/L (see timeseries figure), likely limiting the abundance of cold-water aquatic species.

	1300E	900W
January	1.41	1.92
February	1.73	1.93
March	0.86	0.63
April	0.68	0.64
May	0.78	0.64
June	1.48	0.85
July	2.00	0.81
August	2.14	0.98
September	1.99	0.94
October	2.05	1.70
November	1.86	1.07
December	1.62	1.67

Table A.4.10: Mean monthly Nitrate-N values (mg/L) at Red Butte Creek sites. Nitrate values are on average slightly lower at the 900W site compared to 1300E, but during isolated events, Nitrate-N spikes much higher at 900W than at 1300E.